

AD-A170 422

PAI-FR-0119-2

11

COWBOY TRAILS:  
ANALYSIS OF GAUGE RECORDS FOR PEAK VELOCITY  
AND WAVESPEED

James W. Workman

John G. Trulio

May 1985

DTIC  
ELECTE  
JUL 29 1986  
S B D

SPONSORED BY DEFENSE ADVANCED RESEARCH PROJECTS AGENCY (DoD)  
DARPA Order No. 2692/14, 16, 18, 19 and 20  
Under Contract No. DNA001-80-C-0119

Monitored By: Defense Nuclear Agency (SPTD)  
Washington, D. C. 20305-1000

DTIC FILE COPY

PHYSICS APPLICATIONS, INCORPORATED

PAI

DISTRIBUTION STATEMENT A  
Approved for public release  
Distribution Unlimited

930 South La Brea Avenue, Suite 2  
Los Angeles, California 90036  
(213) 857-5578

86 7 28 168

UNCLASSIFIED

SECURITY CLASSIFICATION OF THIS PAGE (When Data Entered)

REPORT DOCUMENTATION PAGE		READ INSTRUCTIONS BEFORE COMPLETING FORM
1. REPORT NUMBER	2. GOVT ACCESSION NO.	3. RECIPIENT'S CATALOG NUMBER
4. TITLE (and Subtitle) Cowboy Trails: Analysis of Gauge Records for Peak Velocity and Wavespeed		5. TYPE OF REPORT & PERIOD COVERED FINAL REPORT 1 May 1983 - 10 May 1985
7. AUTHOR(s) J. W. Workman J. G. Trulio		6. PERFORMING ORG. REPORT NUMBER PAI-FR-0119-2
9. PERFORMING ORGANIZATION NAME AND ADDRESS Physics Applications, Inc. 930 South La Brea Avenue Los Angeles, California 90036		8. CONTRACT OR GRANT NUMBER(s)  DNA001-80-C-0119
11. CONTROLLING OFFICE NAME AND ADDRESS Defense Advanced Research Projects Agency GSD/DSO 1400 Wilson Boulevard Arlington, Virginia 2209		10. PROGRAM ELEMENT, PROJECT, TASK AREA & WORK UNIT NUMBERS Project No. DARPA No. 2692/14, 16, 18, 19 & 20 Program CODE OD60/OF10/1D60
14. MONITORING AGENCY NAME & ADDRESS (if different from Controlling Office) Headquarters Defense Nuclear Agency Washington, D. C. 20305 ATTN: SPTD		12. REPORT DATE /ZAI0 10 May 1985
		13. NUMBER OF PAGES 57
		15. SECURITY CLASS. (of this report)  UNCLASSIFIED
16. DISTRIBUTION STATEMENT (of this Report)  APPROVED FOR PUBLIC RELEASE DISTRIBUTION UNLIMITED		15a. DECLASSIFICATION/DOWNGRADING SCHEDULE N/A
17. DISTRIBUTION STATEMENT (of the abstract entered in Block 20, if different from Report)		
18. SUPPLEMENTARY NOTES		
19. KEY WORDS (Continue on reverse side if necessary and identify by block number) Deep Buried Explosion Ground Motion Salt Velocity Inelastic Decay		
20. ABSTRACT (Continue on reverse side if necessary and identify by block number) Ten explosive events in a salt dome near Grand Saline, Texas, comprise the core of the Cowboy Trails program. Seven were driven by single spheres of pelletized TNT weighing from 672 to 850 N, and three by two such spheres detonated simultaneously. The resulting ground-motion records have been analyzed to obtain the time of the first-signal arrival, and peak material velocity, as functions of slant-range, r. Though noise and baseline problems affected 491 of the 514 velocity records obtained, and as-built shot layouts proved		

DD FORM 1 JAN 73 1473

EDITION OF 1 NOV 65 IS OBSOLETE

UNCLASSIFIED

SECURITY CLASSIFICATION OF THIS PAGE (When Data Entered)

20.

difficult to determine, 117 records from single-charge events appeared (with simple corrections) to give credible peak velocities; 368 gave times-of-arrival. Inconsistencies among the records reduced these numbers to 73 and 292, respectively.

The arrival times give a wavespeed of  $4.479 \pm 0.021$  km/s, which differs insignificantly from the Cowboy speed. In addition, with the yield,  $W$ , in kilotons, peak velocities decay with  $r$  according to the expression

$0.24(r/W^{1/3})^{-1.456 \pm 0.048}$  m/s, over the scaled range-interval  $0.38 < r/W^{1/3} < 11.3$

km/kt<sup>1/3</sup>. Thus, peak velocity is nearly twice that observed in Cowboy where the two range-intervals overlap, but it decays at a slightly slower rate.

Most important: The Cowboy Trails data show clearly that peak velocity decays inelastically ( $\propto r^{-1}$ ) even at 7 times the largest previous range of observed radial motion from tamped explosions in dome-salt.

Further study of the velocity gauge to determine the cause of baseline problems and correct for them, plus the application of digital processing procedures, should allow recovery of useful data from the bulk of the flawed records. Independent measurement of displacement (attempted in one of the events considered here) would provide a direct test of correction accuracy.

## TABLE OF CONTENTS

<u>Section</u>		<u>Page</u>
1	INTRODUCTION	4
2	THE EXPERIMENTS	6
3	ANALYSIS OF THE GROUND MOTION DATA	11
	3.1 THE DATA	11
	3.1.1 Evaluation of Velocity Records	16
	3.1.2 Geometric Correction of Data	18
	3.2 COMPARISON OF SINGLE-CHARGE GROUND MOTION DATA WITH COWBOY AND SALMON	24
	3.3 PROPAGATION SPEED OF FIRST ARRIVALS	32
4	ANOMALOUS VELOCITY GAUGE SIGNALS	34
	4.1 BASELINE DRIFT	36
	4.2 NOISE	43
5	CONCLUSIONS AND RECOMMENDATIONS	45
	REFERENCES	49
<u>Appendix</u>		
A	THE PLANNED COWBOY TRAILS PROGRAM	51

## LIST OF ILLUSTRATIONS

<u>Figure</u>		<u>Page</u>
1	Ground Motion Instrumentation Stations for the Cowboy Trails Events.	8
2	Plan View of the Ground-Zero Region Showing Charge Locations (★) for the Cowboy Trails Ground Motion Events.	10
3	Typical Velocity Records from the Bell & Howell Electronically Integrating Piezoelectric Accelerometers.	13
4	Representative Records from the Cowboy Trails Accelerometers.	14
5	Raw Signals Obtained in Event III from the Two Functioning Dropweight Displacement Gauges.	15
6	Dependence of Peak Velocity on Scaled Slant Range.	23
7	Comparison of Linear Regression Fits to Peak Velocity, Range Data from Cowboy Trails, Cowboy and Salmon.	25
8	Linear Regression Lines for Peak Radial Velocity as a Function of Scaled-Range for Each of the Single-Charge Cowboy Trails Events.	28
9	Cowboy Trails: Time-of-Arrival, Range Data.	35
10	Simplified Schematic Diagram of the Bell & Howell Velocity Gauge.	37
11	Schematic of the Bias Nulling Circuit for the Bell & Howell Velocity Gauge.	37
12	Comparison of Observed and Calculated response of a Bell & Howell Velocity Gauge to an Observed Acceleration Pulse.	40
13	Observed Response of a Bell & Howell Velocity Gauge During Overloading of the Accelerometer Stage.	42
14	Spikey 60 HZ Noise in a Cowboy Trails Ground Motion Record.	44
A	Overall Plan for Salt Dome Experiments	56

LIST OF TABLES

<u>Table</u>		<u>Page</u>
1	Cowboy Trails Ground Motion Events	9
2	Classification of Cowboy Trails Velocity Gauge Records from Single-Charge Events	17
3	Peak Velocity, Range, and Geometric Correction Factor Data for 117 Records	19.
4	Linear Regression Fit Parameters for $U_{\max} = AR^{-n}$	29
5	Properties of Linear Regression Fits to Time-of-Arrival, Range Data ( $r, t_a$ )	33
6	Comparison of Theoretical and Measured Response of the Bell & Howell Integrator Circuit	39

Accession For	
NTIS GRANT	<input checked="" type="checkbox"/>
DTIC TAB	<input type="checkbox"/>
Unannounced	<input type="checkbox"/>
Justification	
By _____	
Distribution _____	
Availability Codes	
Dist	Avail. and/or Special
<b>A-1</b>	



## SECTION 1

### INTRODUCTION

Careful analysis of ground-motion data from the 5.3-kt Salmon nuclear event<sup>1</sup> and the series of tamped chemical explosive events conducted during the Cowboy program<sup>2</sup> has raised basic questions about the seismic-wave sources produced by explosions in salt, and about the properties of the explosive - pelletized TNT ("Pelletol") - used in the Cowboy experiments<sup>3</sup>. Specifically:

1. Decay of peak velocity and peak displacement with slant range show that salt behaved in a markedly inelastic way out to the largest scaled ranges instrumented in Salmon ( $0.487 \text{ km/kt}^{\frac{1}{3}}$ ) and Cowboy ( $5.744 \text{ km/kt}^{\frac{1}{3}}$ ). At what range and amplitude does deformation become elastic (i.e., far-field peaks  $\propto \hat{R}^{-1}$ )?
2. Wave propagation can be linear without being elastic. The Salmon and Cowboy measurements don't permit linear inelastic behavior to be identified, but seismic theory assures us that at "low enough" amplitudes, geo-materials deform in linear fashion. At what slant range does deformation become linear in dome-salt, and what does the explosively generated linear source look like?
3. If Pelletol releases the energy usually attributed to TNT, then the curves of peak velocity and displacement vs. range for Cowboy lie below those for Salmon. What is the correct energy release for Pelletol charges, tamped in dome salt?
4. With what accuracy does simple scaling apply to motion from tamped explosions in salt?

The four-Phase Cowboy Trails program was undertaken under Defense Advanced Research Projects Agency (DARPA) sponsorship to

answer these questions. Phases I and II were conducted to determine the energy release of tamped chemical explosive charges in dome-salt, by measuring the resulting cavity volumes<sup>4,5</sup> - and also to evaluate simple scaling rules in terms of those volumes. Phases III and IV of the Cowboy Trails program were designed i) to find where the response of dome-salt to a burst in it becomes sensibly linear, and what the motion is like there, ii) to locate any transition from inelastic to elastic propagation of outgoing signals, and iii) to determine the accuracy of simple scaling rules. Appendix A contains a detailed account of the program plan.

Peak material velocity in fields driven by single spherical charges has been taken so far as the criterion for elastic propagation: At far ranges (i.e., where distance to shot-point is  $\gg$  wavetrain-length from first arrival to peak velocity) peak velocity would decay inversely with slant range in a homogeneous, isotropic elastic medium. As for evaluating the rules of simple scaling, it suffices to compare simply-scaled properties of fields produced by bursts of as widely different yield as possible. In this program, measurements were made of the sizes and shapes of cavities left by chemical charges weighing as little as 20-30 gm; by contrast, cavity measurements are available from bursts as large in yield as Salmon. As regards scaling of motion and its Fourier components, extensive ground-motion data were acquired in this program for charges weighing  $\sim 890$  N; again, comparable data extend to yields as high as Salmon's, so that pertinent yields span almost a factor of forty in the scale of time and distance. In the matter of source linearity, no comparisons with earlier events are needed (and there are no relevant in-situ measurements from earlier events in dome salt). Rather, the measure of linearity is the accuracy of superposition. Thus, the program included events in which two spherical charges at various separation-distances were simultaneously detonated, so that the resulting superposed motions (which were measured)

could be compared with single-charge sums.

In view of Cowboy data, the effects of principal interest in this program were sought at greater scaled ranges than those of prior free-field measurement in salt. Hence, comparisons with Salmon, especially, could be made only at the smaller of the ranges observed in these shots. Other complications stem from a) the use of a dome not previously employed for ground-motion experiments, b) use of spherical charges rather than Cowboy-like-cylinders, and c) the exclusion of Pelletol from the smallest bursts of the program (due to its large grains). The logical scheme for evaluating these non-ideal factors one by one is rather intricate; Appendix A goes into its details.

## SECTION 2

### THE EXPERIMENTS

The planned program of ground motion experiments<sup>6</sup> at the Morton Salt Company's Kleer Mine near Grand Saline, Texas, included i) an event with a single spherical charge at the center of the instrumentation array (Event III, comprising Phase III of the program), and ii) a series of three charge-pair events (Events IV-1, IV-2, and IV-3, comprising Phase IV) with charges located symmetrically about the main line of ground-motion instruments.

Instrumentation for the Phase III and IV events consisted of a) 68 velocity gauges and three accelerometers aligned with the  $r$ ,  $\theta$ , and  $\phi$ -directions of a spherical coordinate system with origin at the Event III charge-center, and b) 17 accelerometers and 7 two-axis displacement gauges aligned with the  $R$ ,  $Z$ ,  $\phi$ -directions of a cylindrical coordinate system with symmetry axis

passing vertically through the Event III charge center. The spherically aligned gauges were deployed at eleven slant ranges along four lines (denoted A, B, C and D) corresponding to rays from the center of a regular tetrahedron (the Event III charge) through its vertices, as shown in Figure 1. The velocity gauges, which formed almost all of the primary gauge-array, were electronically integrating, Bell-and-Howell piezoelectric accelerometers of three types: Model 4-155-0122 for the closest-in-stations, Model 4-155-0111 at one intermediate range, and Model 4-155-0129 for the larger slant ranges. Sunstrand Model 305B servo accelerometers replaced the tangential ( $\phi$ ) velocity gauges at stations 11, 12, and 13 on the A-line (hence denoted A11, etc.). Two types of accelerometer were used in the back-up ground-motion array along line A: Columbia Research Laboratories Model 904-PC at stations 3, 4 and 5, and Columbia Research Laboratories Model 3029 adjacent to stations 5, 6, 7, 9, 11, 12 and 13. The two-axis displacement gauges (experimental free-fall gauges being developed by PAI<sup>7</sup>) were installed at stations A3, A4 and A5, B3 and B5, C3, and D5 for use only in Event III. Under separate contract, S-Cubed fielded surface seismometers for some of the events<sup>8</sup> and Stanford Research Institute fielded Flatpak gauges to measure stresses<sup>9</sup> in Event III near the charge.

Delays in reaming spherical cavities for charge placement, problems in demonstrating the safety of drilling deeper than 177 m below the working-level floor, and misfires in the charge-pair events led to the measurement of ground motion for the ten events (in firing sequence) in Table. 1.

Charge locations for the ground motion events are shown in Figure 2. Nominal charge weight was 890N (200 lb) but actual charge weights varied from 672N to 850N (151 to 191 lbs).<sup>10</sup> Four

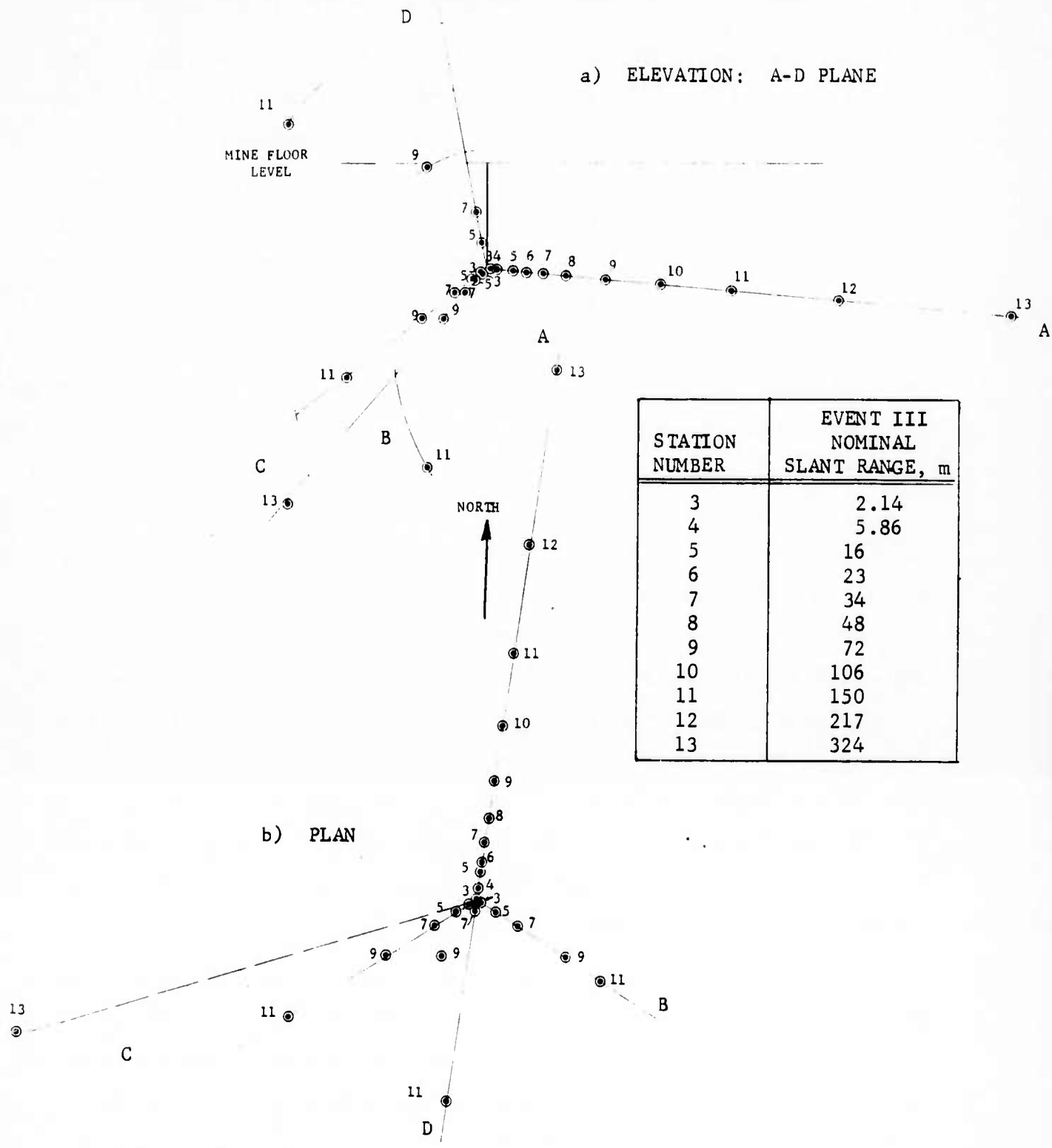


Figure 1. Ground Motion Instrumentation Stations for the Cowboy Trails Events. Except as noted canisters contained three orthogonally oriented ( $r, \theta, \varphi$ ) velocity gauges. Accelerometers were substituted for  $\varphi$ -velocity gauges at Stations A11, A12 and A13. On lines B, C and D (which contain only odd numbered stations) canisters at Stations 5, 9 and 13 contained only  $r$  and  $\theta$  velocity gauges. Radial ( $R$ ) accelerometers were installed along line A at Stations 3, 4, 5, 6 and 7, an  $R, Z$ -pair at Station 9 and orthogonal triads ( $R, Z, \varphi$ ) at Stations 11, 12 and 13. No gauges were installed at B13, D3, or D13.

TABLE 1

## Cowboy Trails Ground Motion Events

Firing Sequence Number	Event	Charge Weight Newtons	As-Built Charge Location		Firing Date	
			South, ft.	East, ft. Depth, ft.		
1	IV-1.0	734.0	787.6	1828.52	344	12 Feb 1983
2	II-8	671.7	707.82	1853.41	40	18 Mar 1983
3	IV-1.1	720.6	796.01	1808.23	335.5	23 Mar 1983
4	II-7	734.0	912.41	1992.18	580	13 Apr 1983
5	IV-1.2	a	763.61	1830.02	99	18 Apr 1983
		b	747.3	1412.56	99	
6	IV-2.0	734.0	886.25	1637.95	238	20 Apr 1983
7	IV-2.1	734.0	872.69	1552.85	238	21 Apr 1983
8	III	849.6	916.44	1597.62	205	23 Apr 1983
9	IV-2.2	a	866.75	1649.36	155	28 Apr 1983
		b	689.5	1549.36	155	
10	IV-3	a	906.77	1600.55	215	29 Apr 1983
		b	676.1	1582.94	215	

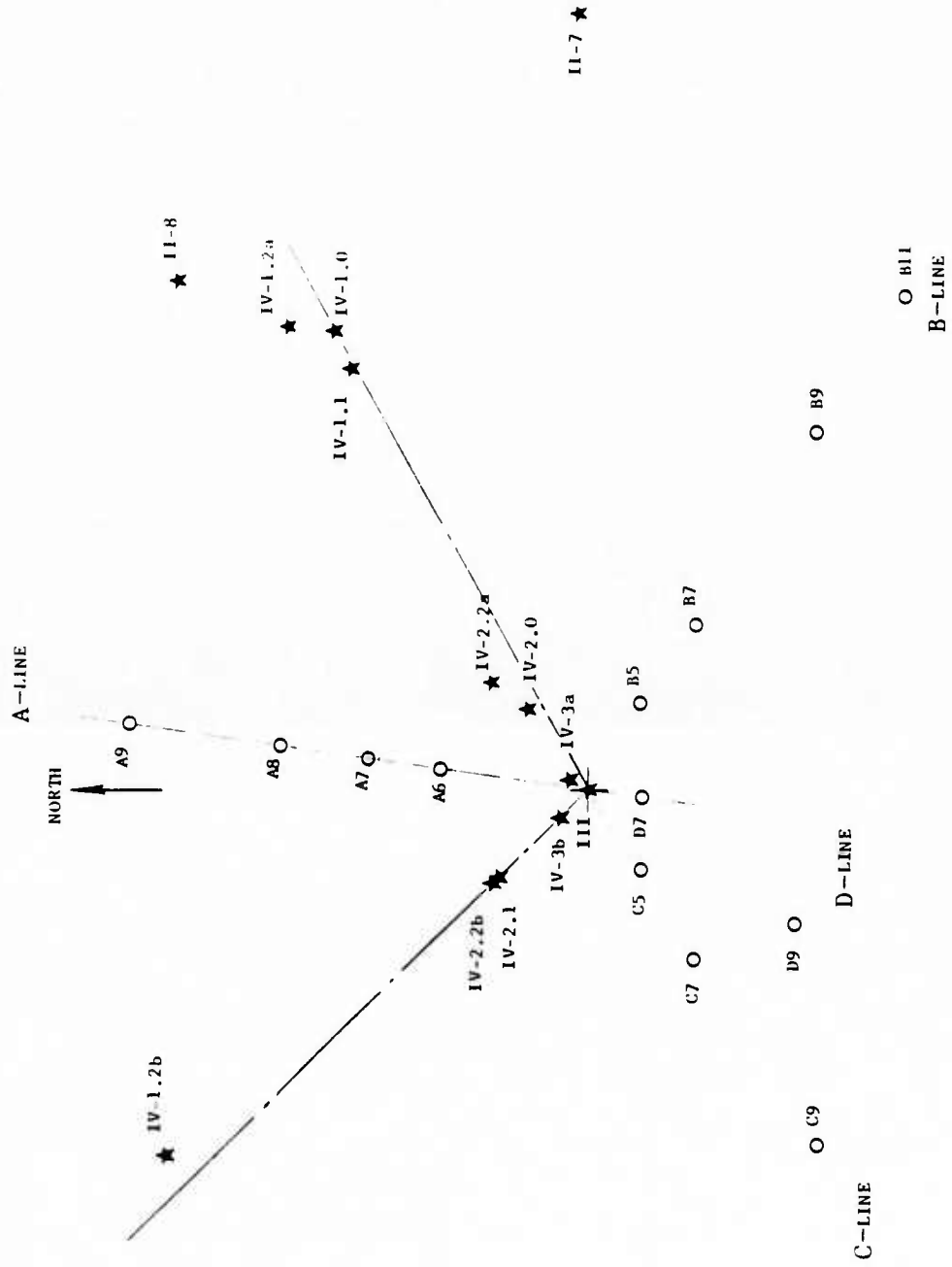


Figure 2. Plan View of the Ground-Zero Region Showing Charge Locations (★) for the Cowboy Trails Ground Motion Events. Open circles indicate a number of instrument stations to facilitate comparison with the instrumentation layout of Figure 1. Close-in gauge locations (A3, A4, A5, B3, C3, and C5) have been omitted for clarity

of the single-charge events (IV-1.0, IV-1.1, IV-2.0 and IV-2.1) were the result of misfires during attempts to simultaneously detonate symmetric charge pairs. One charge, IV-1b failed to detonate in events IV-1.0 and IV-1.1, the first two attempts to fire the dual charge-pair event IV-1. It was destroyed by sympathetic detonation during cleanup operations.

### SECTION 3

#### ANALYSIS OF THE GROUND MOTION DATA

Up to now, the main goals of data analysis, have been i) to assess the credibility of the data, noting where ground motion signals were affected by anomalies, ii) to establish gross properties of the ground motion field (velocity of first-arriving signal, decay of peak particle velocity with range) from the credible data, and iii), by examining questionable data, to determine probable causes of errors and anomalies along with means of removing them - thereby recovering useful information.

##### 3.1 The Data

Data from the ground-motion instrumentation array was recorded in analog form. Subsequently, copies of the master analog tapes were used to generate digital records covering about 0.2 second before and 1.0 second after zero time for each event. After analog-to-digital conversion and recording, plots of the digital pulses were generated (These appear in Appendices B through K of Ref. 7).

The completed ground motion instrumentation array could have produced 680 velocity gauge records, 200 accelerometer records

and 14 displacement records in the ten events of Table 1. Attrition due to gauge or cable failure, connector corrosion, late installation and digital record processing problems, accounted for the loss of 141 velocity, 68 acceleration and 12 displacement records. Pulses representative of the 539 velocity records, 132 accelerations and 4 displacement gauge records reported in Ref. 7 are shown in Figures 3, 4 and 5. The pulses in Figure 3, parts b-f, show that noise and baseline instability were significant problems in recording velocities. The accelerometers, Figure 4, show significant ringing and some baseline problems. The displacement records, Figure 5, are noisy and the non-linear cross-axis-coupled response of the gauge adds to the difficulty of their interpretation.

Only 363 velocity records, 87 accelerations and 2 displacements are applicable to determining the characteristics of a spherically symmetric field of motion. The non-radial velocity gauges from Event III can't be used to infer radial motion. Likewise, since signals from the charge-pairs cannot be separated reliably into single-charge signals, records from Events IV-1.2, IV-2.2 and IV-3 are not pertinent. The number of useful records was reduced still further by some technical problems with the digital pulse records. These problems arose during attempts to read the digital ground motion records, and verify them by comparison with what should have been the same pulses plotted earlier (Ref. 7). A few files were unreadable. Identification and scaling from "digital bit count" to measured physical amplitude was uncertain or not possible for many others; no directory was provided in Reference 7 for the tape containing most of the digitized acceleration records. This left the plots in Ref. 7 as the primary means of defining the ground motion records. Since the majority of the digitized accelerometer records were available only in graphical form, they were not integrated to check the relative accuracy of

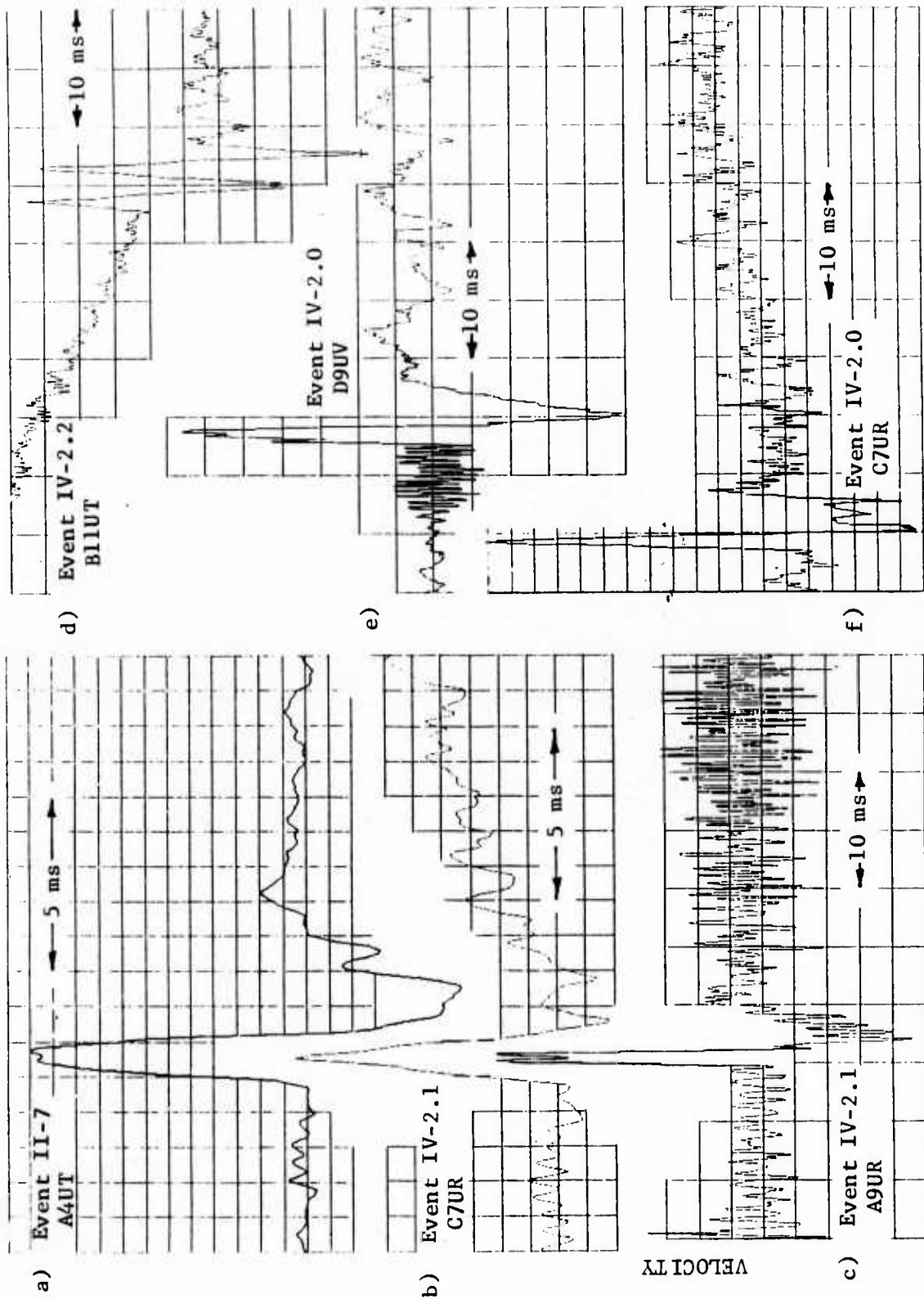


Figure 3. Typical Velocity Records from the Bell & Howell Electronically Integrating Piezoelectric Accelerometers. Noise and baseline problems which affected nearly all the data are evident in records b) through f).

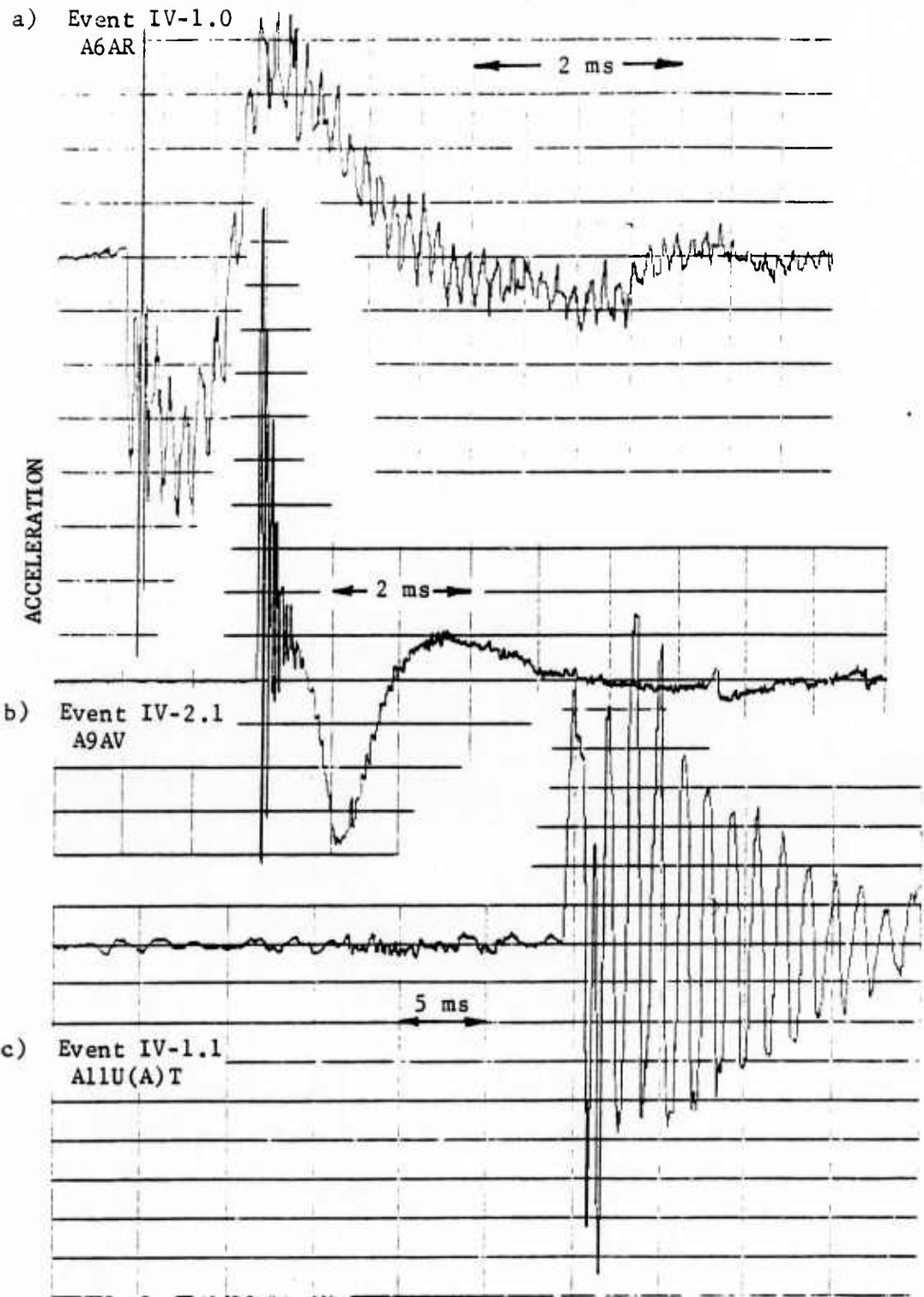


Figure 4. Representative Records from the Cowboy Trails Accelerometers. Traces a) and b) are from Columbia Research Laboratories Type 3029 piezoelectric accelerometers in the back-up array. Trace c) is from one of the Sunstrand Model 305B servo-accelerometers substituted for a transverse ( $\psi$ -component) velocity gauge in the primary ground motion instrumentation array.

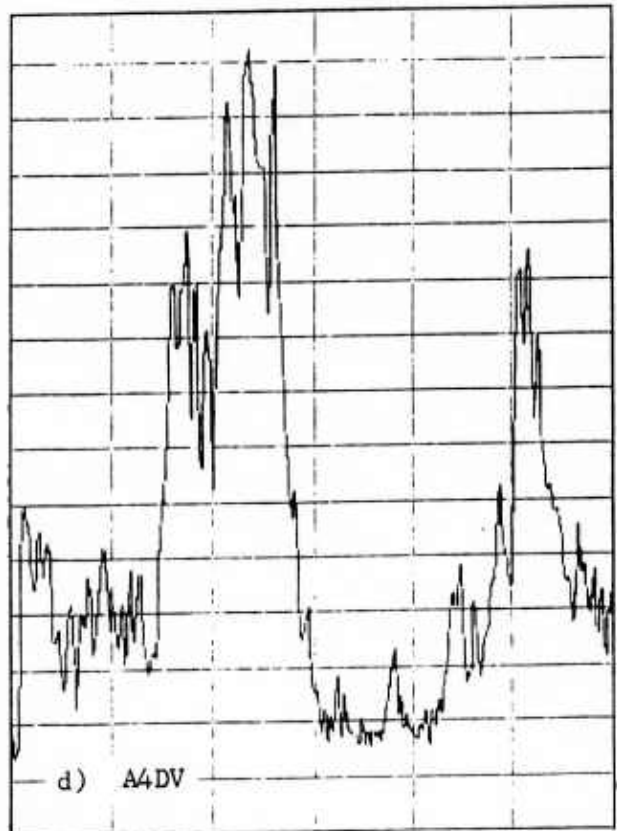
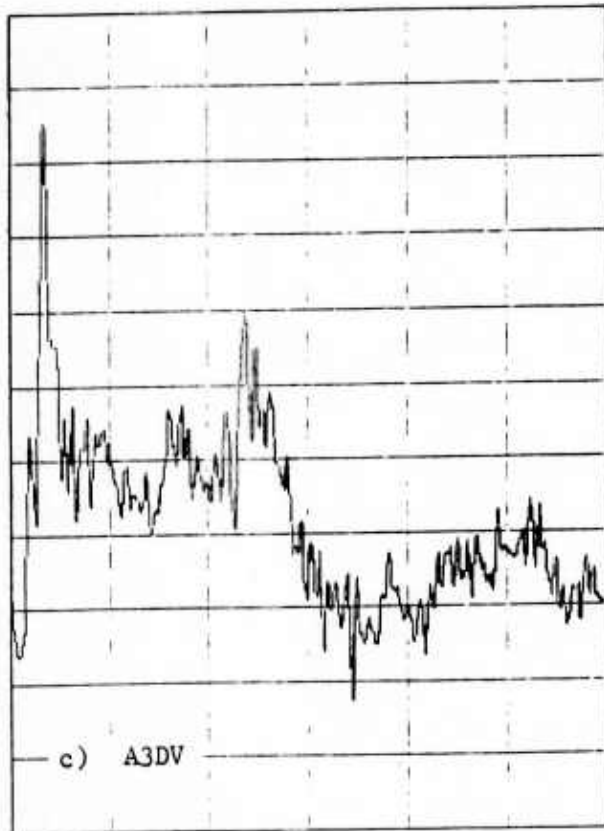
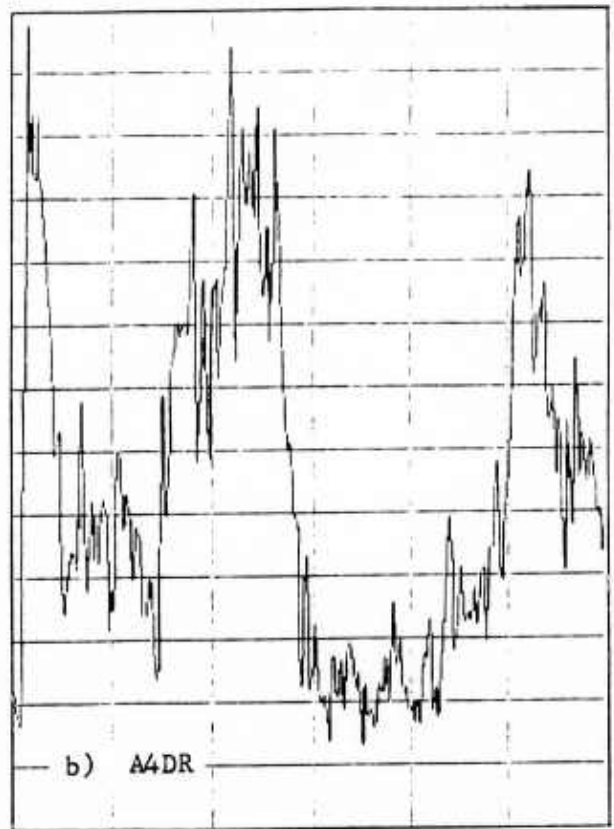
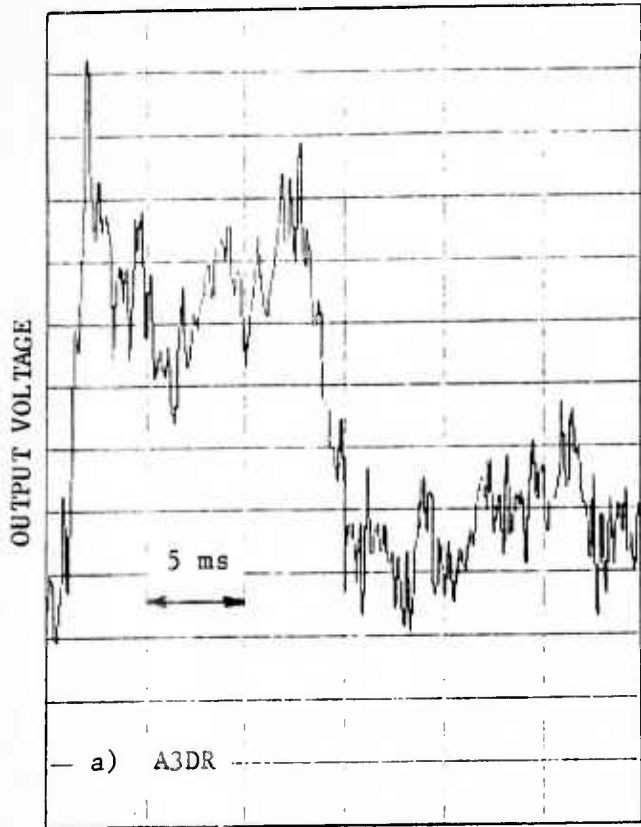


Figure 5. Raw Signals Obtained in Event III from the Two Functioning Dropweight Displacement Gauges. Displacement gauges were installed at 7 stations - A3, A4, A5, B3, B5, C3, and D5 - but corrosion rendered most inoperable before Event III was fired.

accelerometers and velocity gauges. The displacement records were of limited value because of the lack of corresponding velocity records and incomplete calibration. Attention was therefore focused on the velocity gauge records from single charge events.

### 3.1.1 Evaluation of Velocity Records

Each of the velocity pulse records was scrutinized to establish whether a signal reliable through peak velocity had been obtained. Records were classified according to the defects they contained: Noise, baseline drift (which includes offset and low-frequency oscillation), and other, such as clipping of peaks, strange pulse-shape and gauge failure. Of a possible set of 680 velocity records from all 10 events, 141 records were blank or unusable and 25 that reported were oriented to record only non-radial motion. Furthermore, while 7 of the 514 records of potential use appear to require no significant correction, 16 suffer from defects that can't be associated clearly with either noise or baseline drift. The other 491 records exhibit noise, baseline drift, or both, severe enough to interfere with their interpretation. Baseline drift is the sole artifact that appears to require correction in 52 of those records and 190 need to be corrected for noise alone, while 249 need correction for both drift and noise. In preparing this report, 173 records - the 7 clean records and 166 records we felt could reasonably be corrected now - appear to provide signals good through peak velocity; however, better knowledge of the gauges' workings might change our reading even of that subset. Detailed results of the screening of records from the 7 single-charge events are given in Table 2.

All records were subjected to a second review to assure that the pulse plot identification, digital record file number and scale factor were consistent and correct. At the same time, it was judged that the 56 records from charge-pair events, in spite of

TABLE 2

CLASSIFICATION OF COWBOY TRAILS VELOCITY GAUGE RECORDS  
FROM SINGLE-CHARGE EVENTS

Record Class	II-7	II-8	III*	IV-1.0	IV-1.1	IV-2.0	IV-2.1	Total	Defective	Good V <sub>max</sub> **
	13	9	10	14	9	11	9			
No Report***								75		
Reporting Clean	1	1	1	1	1	-	-	5	-	5
Noise	32	28	3	24	23	12	12	134	78	56
Baseline and Noise	17	28	9	19	28	36	39	176	133	43
Baseline	2	2	2	7	7	9	8	37	24	13
Other	3	1	2	-	3	-	-	8	8	-
Total Reports	55	59	17	54	59	57	59	360		
Defective	37	36	13	41	37	38	41		243	
Good V <sub>max</sub> **	18	23	4*	13	22	19	18			117
Total Channels	68	68	27*	68	68	68	68	435		

\* An aiming error in canister D9 allowed gauge D9UV to measure the radial velocity in Event III, increasing the number of pertinent channels to 27 and the number of records good through peak to 4. Of the 41 channels incapable of measuring radial velocity (not included here), 16 gave no report.

\*\* Includes clean records and records corrected by inspection for simple baseline and noise defects.

\*\*\* No record is included in Reference 7, Appendices B through K.

providing signals otherwise good through peak velocity, could not be reliably separated into single-charge signals. Determination of peak velocity as a function of range was thus limited to the 117 good records (5 clean, 112 corrected) from single-charge events listed in Table 3.

Scale factor errors were present in plots for 12 of the good records for single-charge events and identification ambiguities affected 20 records (one of them also affected by a scale factor error). The identification ambiguity of 18 records was resolved by reading and replotting the digital records. Scale factor errors consisting of transposition of digits, substitution of a factor for a different gauge, or amplitude shift by an integral power of 10, were corrected.

### 3.1.2 Geometric Correction of Data

Since the velocity gauge array was designed to measure the spherically symmetric field of motion from Event III and latitudinal and longitudinal departures from symmetry, the motions recorded for all other events must be adjusted to account for event-to-event changes in charge location. To obtain a description of the spherically symmetric radial motion, the signal  $V_i$  measured by a gauge pointing in some arbitrary direction  $\hat{e}_i$  must be related to the radial velocity  $\vec{V}_r = V_r \hat{e}_r$ .

The particle velocity at any point is:

$$\vec{V} = V_R \hat{e}_R + V_V \hat{e}_V + V_T \hat{e}_T \quad (1)$$

where  $\hat{e}_R$ ,  $\hat{e}_V$ , and  $\hat{e}_T$  are the orthogonal unit vectors pointing in the directions of the sensitive axes of the velocity gauges.

TABLE 3

Peak Velocity, Range, and Geometric Correction Factor Data for 117 Records

Event	Gauge	Scaled		U <sub>max</sub> , m/s	α	Event	Gauge	Scaled		U <sub>max</sub> , m/s	α
		Range, m	Range, km/kt					Range, m	Range, km/kt		
11-7	431	165.2	4.2500	1.8274	1.550	11-1	441	30.9	2.0677	0.954	1.301
11-7	441	155.0	4.1971	0.615	1.290	11-1	451	75.9	1.9423	0.970	1.290
11-7	450	154.0	4.1710	0.744	1.460	11-1	461	40.7	1.8763	0.855	2.170
11-7	474	163.5	4.1370	0.630	3.170	11-1	471	64.8	1.7350	1.400	4.650
11-7	473	153.5	4.1370	0.743	1.460	11-1	472	40.8	1.7751	1.111	1.950
11-7	4114	203.7	5.1816	0.349	1.550	11-1	484	69.5	1.7520	1.0550	1.0850
11-7	4114	203.7	5.1816	0.286	1.790	11-1	494	63.5	1.7520	1.520	1.940
11-7	4121	243.0	6.3320	1.150	2.241	11-1	494	72.2	1.8477	1.445	2.300
11-7	4134	337.9	8.5320	0.141	1.140	11-1	4114	122.1	3.1233	0.434	1.210
11-7	434	164.3	4.1790	0.7520	1.270	11-1	4134	203.6	7.2575	0.124	1.030
11-7	434	152.6	3.8820	0.446	1.230	11-1	4144	76.0	1.9440	0.110	2.371
11-7	434	152.6	3.8820	0.446	2.600	11-1	4154	117.7	2.7560	0.459	1.530
11-7	434	152.6	3.8820	0.446	2.330	11-1	4164	117.7	2.7560	0.305	1.530
11-7	434	177.7	4.5190	0.450	1.210	11-1	4174	117.7	2.7560	1.219	27.591
11-7	434	177.7	4.5190	0.339	2.770	11-1	4184	139.1	3.5600	0.431	1.131
11-7	434	150.3	3.8820	0.171	1.240	11-1	4194	139.1	3.5600	0.436	2.391
11-7	434	150.3	3.8820	0.171	1.610	11-1	4204	377.9	9.6680	0.033	1.021
11-7	434	150.3	3.8820	0.171	2.037	11-1	4214	94.4	2.4150	0.533	1.421
11-7	434	150.3	3.8820	0.171	1.550	11-1	4224	107.6	2.7940	0.241	1.241
11-7	434	150.3	3.8820	0.171	2.500	11-1	4234	133.1	3.9160	0.799	3.403
11-7	434	150.3	3.8820	0.171	2.780	11-1	4244	213.0	5.5750	0.124	1.443
11-7	434	150.3	3.8820	0.171	1.000	11-1	4254	17.0	0.3320	0.500	2.070
11-7	434	150.3	3.8820	0.171	1.300	11-1	4264	14.9	0.3790	1.680	3.351
11-7	434	150.3	3.8820	0.171	1.540	11-1	4274	14.9	0.3790	1.020	1.680
11-7	434	150.3	3.8820	0.171	1.300	11-1	4284	13.3	0.4660	0.630	1.600
11-7	434	150.3	3.8820	0.171	1.700	11-1	4294	13.3	0.4660	0.750	2.650
11-7	434	150.3	3.8820	0.171	1.410	11-1	4304	61.8	1.5720	1.270	1.930
11-7	434	150.3	3.8820	0.171	1.480	11-1	4314	61.8	1.5720	1.421	5.870
11-7	434	150.3	3.8820	0.171	1.420	11-1	4324	138.8	3.5291	0.210	15.410
11-7	434	150.3	3.8820	0.171	3.020	11-1	4334	312.5	7.9450	0.384	1.000
11-7	434	150.3	3.8820	0.171	1.060	11-1	4344	17.7	0.4490	0.740	2.540
11-7	434	150.3	3.8820	0.171	1.920	11-1	4354	139.3	3.5420	1.450	80.550
11-7	434	150.3	3.8820	0.171	1.000	11-1	4364	19.7	0.5000	0.590	1.290
11-7	434	150.3	3.8820	0.171	1.500	11-1	4374	46.5	1.1820	0.752	1.060
11-7	434	150.3	3.8820	0.171	1.540	11-1	4384	83.1	2.1130	0.230	5.510
11-7	434	150.3	3.8820	0.171	1.000	11-1	4394	333.0	3.4680	0.132	1.000
11-7	434	150.3	3.8820	0.171	4.370	11-1	4404	31.6	0.8030	0.230	1.100
11-7	434	150.3	3.8820	0.171	3.050	11-1	4414	93.5	2.3600	0.640	2.249
11-7	434	150.3	3.8820	0.171	1.139	11-1	4424	163.0	4.1950	0.227	1.300
11-7	434	150.3	3.8820	0.171	1.101	11-1	4434	155.0	4.1950	0.130	16.970
11-7	434	150.3	3.8820	0.171	1.101	11-1	4444	19.0	0.4580	1.930	4.430
11-7	434	150.3	3.8820	0.171	1.101	11-1	4454	20.6	0.5230	0.530	2.490
11-7	434	150.3	3.8820	0.171	1.101	11-1	4464	20.6	0.5230	0.530	2.490
11-7	434	150.3	3.8820	0.171	1.101	11-1	4474	28.3	0.7200	0.200	1.930
11-7	434	150.3	3.8820	0.171	1.101	11-1	4484	82.3	1.5830	0.170	1.040
11-7	434	150.3	3.8820	0.171	1.340	11-1	4494	109.6	3.5250	0.459	1.110
11-7	434	150.3	3.8820	0.171	1.340	11-1	4504	312.1	7.9560	0.112	1.30
11-7	434	150.3	3.8820	0.171	1.340	11-1	4514	30.6	0.8500	0.120	1.940
11-7	434	150.3	3.8820	0.171	2.130	11-1	4524	49.2	1.2510	0.270	3.40
11-7	434	150.3	3.8820	0.171	1.260	11-1	4534	130.5	3.9280	0.775	7.630
11-7	434	150.3	3.8820	0.171	1.260	11-1	4544	30.6	0.5230	0.730	2.430
11-7	434	150.3	3.8820	0.171	1.260	11-1	4554	57.1	1.7050	0.177	1.050
11-7	434	150.3	3.8820	0.171	1.260	11-1	4564	67.1	1.7540	1.540	2.100
11-7	434	150.3	3.8820	0.171	1.260	11-1	4574	111.9	7.9510	0.124	1.430
11-7	434	150.3	3.8820	0.171	1.260	11-1	4584	33.4	0.8530	0.230	1.100
11-7	434	150.3	3.8820	0.171	1.260	11-1	4594	49.7	1.2640	0.230	1.100
11-7	434	150.3	3.8820	0.171	1.260	11-1	4604	49.7	1.2640	0.230	1.100
11-7	434	150.3	3.8820	0.171	1.260	11-1	4614	30.1	2.2920	1.960	1.960
11-7	434	150.3	3.8820	0.171	1.260	11-1	4624	155.5	4.2150	0.517	1.000

The spherical radial velocity is

$$V_r = \hat{e}_r \cdot \vec{V} = V_R(\hat{e}_r \cdot \hat{e}_R) + V_V(\hat{e}_r \cdot \hat{e}_V) + V_T(\hat{e}_r \cdot \hat{e}_T) \quad (2)$$

where  $\hat{e}_r$  is a unit vector pointing along the ray from the charge to the gauge canister. However, for this relationship to be useful here, records for all three components of motion are needed and they must be good through their vector-sum's peak. Because of uncertainties and omissions in the data linking the plots of Reference 7 to the digitized records on magnetic tape, the construction of vector sums was not attempted. Instead, it was assumed that peaks of  $V_R, V_V$ , and  $V_T$  occur simultaneously, i.e., Eq. (1) is assumed valid for combining component peaks.

Inverting Equation 1, leads to a description of the velocity component  $V_i$  measured by a gauge pointing in the direction  $\hat{e}_i$  in terms of the  $r, \theta$ , and  $\varphi$ -components of velocity:

$$\begin{aligned} V_i &= \hat{e}_i \cdot \vec{V} = \hat{e}_i \cdot (V_r \hat{e}_r + V_\theta \hat{e}_\theta + V_\varphi \hat{e}_\varphi) \\ &= V_r(\hat{e}_i \cdot \hat{e}_r) + V_\theta(\hat{e}_i \cdot \hat{e}_\theta) + V_\varphi(\hat{e}_i \cdot \hat{e}_\varphi) \end{aligned} \quad (3)$$

If the field of motion is spherically symmetric ( $V_\theta=0$  and  $V_\varphi=0$ ), Eq. 3 simplifies to

$$V_i = V_r(\hat{e}_i \cdot \hat{e}_r) \quad (4)$$

Radial velocity can then be obtained as follows from single records of motion, when the charge and gauge location are known along with the directions of the sensitive axes of the gauges:

$$V_r = V_i / (\hat{e}_i \cdot \hat{e}_r) = \alpha \cdot V_i \quad (5)$$

where  $\alpha = (\hat{e}_i \cdot \hat{e}_r)^{-1}$  is the geometric correction factor.

If the field of motion produced by a single charge is spherically symmetric and the gauges accurately report free-field motion, then all the estimates of the radial velocity obtained from a given canister will be the same. For a canister with three gauges (records of  $V_R, V_V$ , and  $V_T$ ), Equation 2 will yield one estimate and Equation 5 will provide three. The actual field will be only approximately spherical, the gauges only approximately aligned in the planned directions, the canister motion a bit different than that of the free field, and the gauges slightly (and differently) in error in sensing and reporting the motion. The differences between estimates from a single canister will reflect the combined effects of all these factors (as well as the accuracy of our assumption that component peaks at any station occur simultaneously), and will give a qualitative idea of measurement accuracy. Since several canisters contained only two velocity gauges and few canisters with 3 gauges yielded complete sets of good records, the estimates of radial velocity based on Equation 1 were too few to be of value. To provide an adequate data base and allow uniform treatment of the velocity data, Equation 5 was adopted to define the amplitude of radial velocity for each single-charge event.

Because the description of canister and charge locations given in Ref. 7 is incomplete, additional data were sought from records of telephone conversations and working notes to complete the definition of gauge and source geometry. Although some of the additional data led to conflicts with Ref. 7, a provisional picture of the as-built configuration has been developed. To resolve the conflicts for the moment, it has been assumed that the canister locations of Table 9 with the down-hole survey corrections of Table 10 of Ref. 7 are correct and that survey layouts for the

slant holes<sup>11\*</sup> provide the proper orientation of the slant holes relative to the rays from the Event III charge to the canisters. Where data are missing\*\*, it has been assumed that gauge orientation and location are correct, i.e., unsurveyed holes did not wander from their intended direction.

Using this description of the as-built configuration, the geometric correction factors of Eq. 5 were computed for all gauges for all events. The Event-III factors for all R-velocity gauges were compared with those derived from gauge mounting-block details.<sup>11</sup> This comparison revealed aiming errors of  $28^\circ$  for gauges D9UR and D9UV,  $1.8^\circ$  for gauges C7UR and C7UV, and an indication that the inclination of in-plane slant hole B9 was  $7.2^\circ$ . Since no good records were obtained from B9 gauges, no further effort was made to resolve the question of slant-hole inclination or gauge orientation there. The  $1.8^\circ$  aiming error for the C7 gauges was considered small enough to ignore (errors in corrected peak radial velocities from this source would be less than 7%, and less than 4% in seven of the eight cases where good records were obtained). Geometric correction factors for gauges D9UR and D9UV were recalculated to account for their misorientation.

The geometric correction factors, estimates of radial velocity, slant ranges and yield-scaled slant ranges are listed in Table 3. The peak radial velocity, scaled slant range data for all entries with geometric correction factors (Eq. 5) less than 5 (gauge-axis pointing within  $78.46^\circ$  of ray from charge) have been plotted in Figure 6. Points labelled A through D (A, B and C from Event II-7 and D from Event IV-2.1) are clearly outside reasonable scatter bounds for the remainder of the data. They have been ignored in obtaining the 7-event regression fit shown.

\*The two sets of data imply azimuths for line C, Stations 3-11, that differ by  $\sim 16^\circ$ .

\*\*Despite diligent search and a careful review of all available data, the orientation of in-plane slant hole B-9 remains unknown.

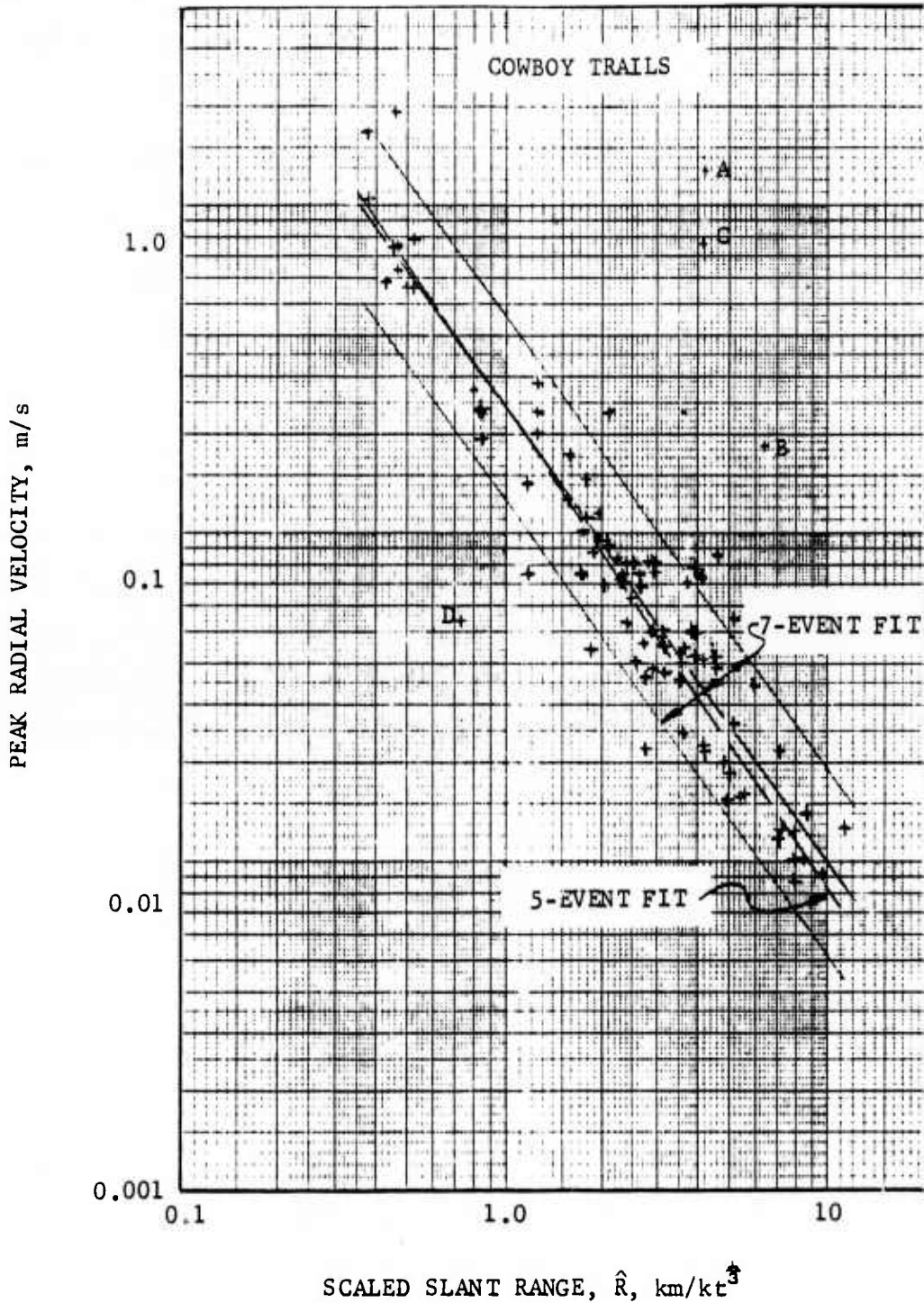


Figure 6. Dependence of Peak Velocity on Scaled Slant Range. Data from 97 gauges in 7 single-charge events gives the linear regression curve:  $U_{\max} = 0.244\hat{R}^{-1.383 \pm 0.050}$  and a 90% confidence band whose limits are in the ratio  $U^+/U^- = 3.67$ . Ignoring the less consistent data from Events II-7 and IV-1.0 left 73 records and the 5-Event fit:  $U_{\max} = 0.239\hat{R}^{-1.456 \pm 0.048}$  with  $U^+/U^- = 3.13$ .

$$V_{\max} = 0.244R^{\hat{-1.383 \pm 0.050}}$$

The 90% confidence limits cover a band whose bounds, top to bottom, are in the ratio 3.67:1. Further study of the data led us to reject the peaks from two events (Section 3.2 below), giving a best estimate somewhat different than this one.

### 3.2 Comparison of Single-Charge Ground Motion Data with Cowboy and Salmon.

Ground motions were measured for two other programs conducted in dome salt: Project Cowboy<sup>2</sup> in the Carey Salt Mine at Winnfield, Louisiana, and Project Dribble<sup>1</sup> in the Tatum salt dome near Hattiesburg, Mississippi. Project Cowboy included 8 tamped shots fired between 17 December 1959 and 9 March 1960 that were comparable to the Cowboy Trails single-charge events. Explosive charges in the series of tamped shots ranged from 20 to 1000 lbs of Pelletol\*<sup>13</sup> (spheroidal pellets of TNT with diameters of about 3/32 inch). Under the conditions for tamped charges in Cowboy and Cowboy Trails, the confinement-dependent energy release of Pelletol has been taken as 3.4 kj/g, the value deduced from the earlier phases of Cowboy Trails.<sup>4</sup>

Data for events 4, 7, 9, 11, 16 and 17 with charges weighing 100 to 1000 lbs were used to obtain the peak velocity/range curve ( $V_{\max} = 0.1456R^{\hat{-1.527}}$ )<sup>14</sup> shown in Figure 7. Velocity-gauge data and integrated accelerometer data from the Salmon event of Project Dribble, a tamped 5.3 kt nuclear detonation fired 22 October 1964 were used to obtain the Salmon curve ( $V_{\max} = 0.1930R^{\hat{-1.9524}}$ ).<sup>14</sup>

Careful review of ground-motion data acquisition systems used in Cowboy<sup>15</sup> and Salmon<sup>1</sup> has shown that the scaled frequency

\*Trojan Corporation's Nitropel, the currently available pelletized TNT explosive, was used in the spherical Cowboy Trails charges. DuPont Pelletol 1 was used in the Cowboy cylindrical charges.

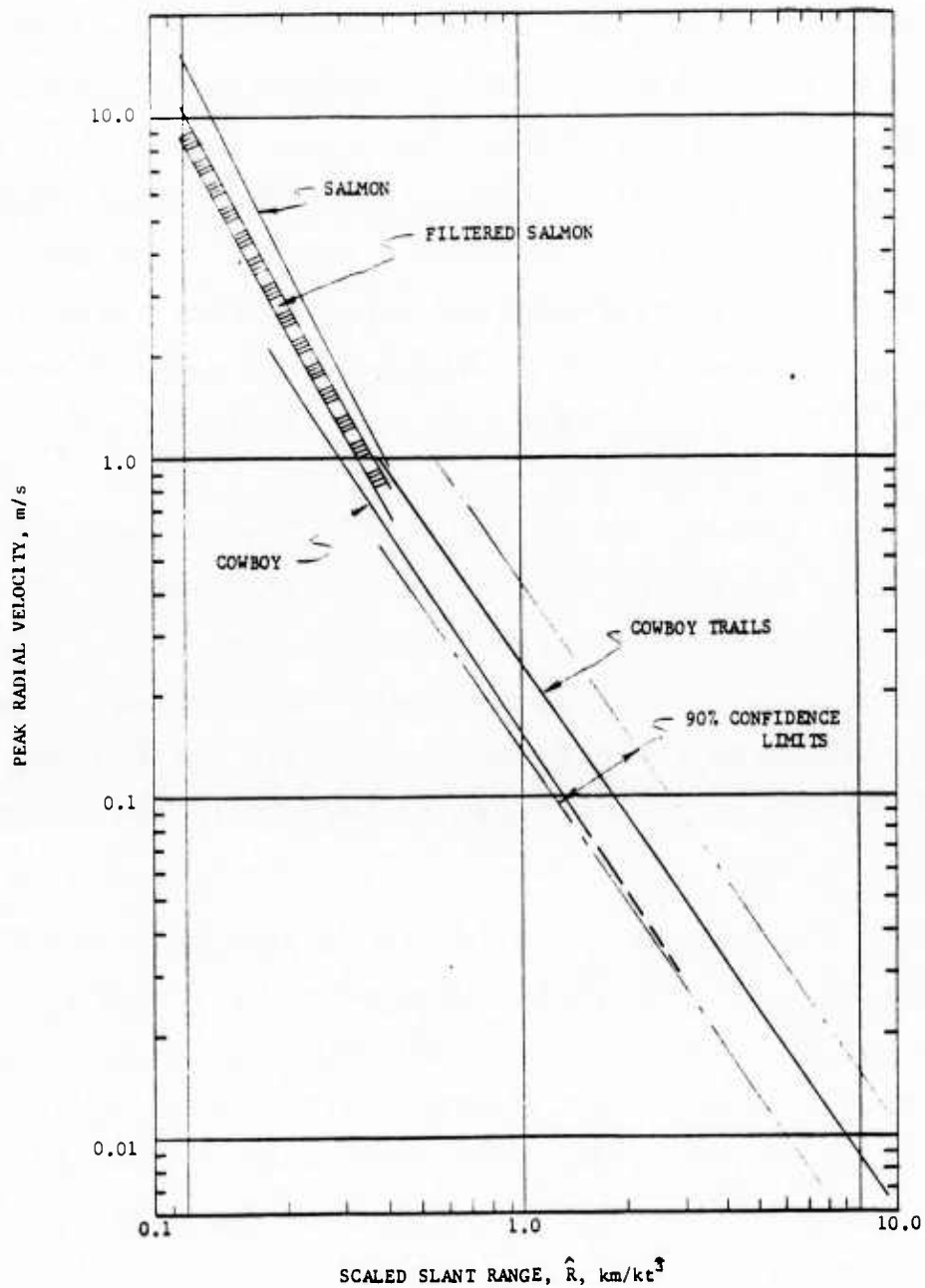


Figure 7. Comparison of Linear Regression Fits to Peak Velocity, Range Data from Cowboy Trails, Cowboy and Salmon. Filtered Salmon data have been passed through a digital filter representing the  $W^3$ -scaled frequency response of the Cowboy data acquisition system. High frequency response is reduced, decreasing both amplitude and the rate of decay with range. Curve for Cowboy is dashed for  $R > 1.61 \text{ km/kt}^3$  where orientation of gauges could not be confirmed.

response of the velocity gauges used in Cowboy is quite low, especially with respect to that for Salmon.<sup>3</sup> Limited frequency response sharply reduces peaks at close-in stations, but the effect decreases with range; higher frequencies decay more rapidly with distance than lower frequencies. As a result the rate of decay of peak velocity with range is decreased by reducing the frequency response of the instrumentation system. Passing Salmon data through digital filters representing the frequency response of the Cowboy velocity gauges scaled to Salmon yield reduced peak velocities by 26 to 41% close-in, depending on the gauge type represented by the filter and by 6 to 23% at the outermost range.<sup>16</sup> The decay-exponent fell from 1.9524 to 1.783 or 1.766 as shown by the curves bounding the shaded region for filtered Salmon in Figure 7. No attempt has yet been made to account for the differences in ground motion from cylindrical (Cowboy) and spherical (Cowboy Trails) charges or for the differences between the frequency response characteristics of velocity gauges used to record Cowboy and Cowboy Trails motions.

The exponent  $n$  for decay of peak velocity with range (1.383) is lower in Cowboy Trails than that observed for both Cowboy (1.527) and Salmon (1.9524;  $1.775 \pm .009$  after filtering to compare with Cowboy). However, 90% confidence limits encompass the regression curves for both Salmon and Cowboy over the scaled range-interval from  $.175 \text{ km/kt}^{\frac{1}{3}}$  to the most distant Cowboy gauge (and our best present estimate of  $n$  is somewhat larger than 1.383; below). Still, Cowboy Trails' peak amplitudes are almost all higher than the Cowboy regression line, which lies just inside the lower 90% confidence bound. Thus, while little overlap occurs in the scaled range-intervals on which ground motion was observed in Salmon and Cowboy Trails ( $0.37 < \hat{R} < 0.42 \text{ km/kt}^{\frac{1}{3}}$ ), it is reassuring to find that the regression line for Cowboy Trails falls between the fits to Salmon and filtered Salmon data.

The comparison of Cowboy Trails with Cowboy presents some puzzles. The combination of higher amplitude but lower rate of decay with range cannot be explained by frequency response differences of the kind demonstrated in comparisons of Cowboy and Salmon. The differences might result from the predominance of Cowboy Trails observations at scaled ranges beyond those used in Cowboy (the log mean range is  $2.465 \text{ km/kt}^{\frac{1}{3}}$ ), where deformation is more nearly elastic, or from systematic errors in single events. In particular, signals from Event II-8, the shallowest shot, may all be contaminated by surface reflection; records for Event II-7, the deepest shot, may all be affected by a suspected, but unconfirmed, error in charge location that overstates the ranges to all stations (Section 3.3). The full set of records may also be affected by superposed noise that overstates all peak values.

Treating good records from each event separately produces the seven regression lines shown in Figure 8, whose parameters are listed in Table 4. An eighth regression line, also shown, fits all the good Cowboy Trails records for scaled ranges less than  $1.61 \text{ km/kt}^{\frac{1}{3}}$  - the largest range at which radial orientation of the Cowboy gauges has been confirmed. The exponents for power-law decay vary from a low of 1.232 for Event IV-1.0 to a high of 1.775 for Event II-7. The 90% confidence-limit bands have widths,  $U^+/U^-$ , varying from 1.22 for Event III to 4.63 for Event II-7. The decay exponents for Events III, IV-2.0, IV-2.1 - the only events yielding good records for  $\hat{R} \leq 1.7 \text{ km/kt}^{\frac{1}{3}}$  (the interval of overlap with Cowboy) - are, respectively, 1.500, 1.522, 1.596 and 1.556. For all intents, they are equal to that for Cowboy (1.527). Amplitudes, however, run from about 1.20 to nearly twice the Cowboy amplitude. Peak velocities from the four events yielding records only for large scaled ranges - Events II-7, II-8, IV-1.0, and IV-1.1 - tend to be high. Their regression lines lie above those for Events III,

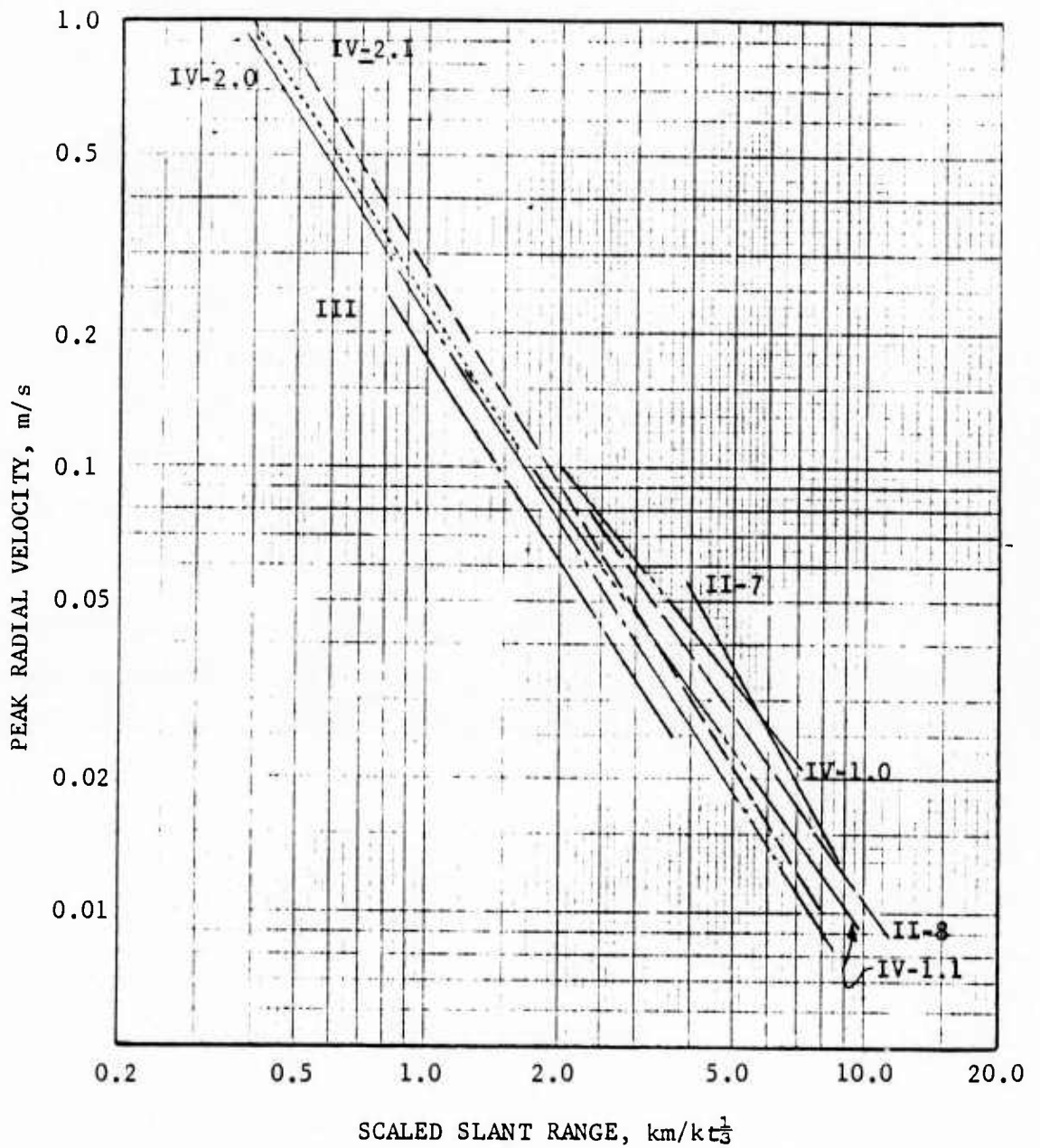


Figure 8. Linear Regression Lines for Peak Radial Velocity as a Function of Scaled-Range for Each of the Single-Charge Cowboy Trails Events. The unlabelled dotted-line at the upper left is the linear regression fit to all Cowboy Trails data in the scaled-range interval covered by both Cowboy and Cowboy Trails,  $0.38 \leq R \leq 1.61 \text{ km}/\text{kt}^{1/3}$ .

TABLE 4

Linear Regression Fit Parameters for  $U_{\max} = \hat{A}R^{-n}$ 

Event	N	A	n	$\delta_n$	90% Confidence Band Width $U^+/U^-$
II-7*	14	0.6124	1.7746	$\pm 0.6267$	4.63
II-8	20	0.2566	1.3923	$\pm 0.1534$	2.52
III	4	0.1779	1.5000	$\pm 0.0542$	1.22
IV-1.0*	10	0.2359	1.2315	$\pm 0.3554$	4.03
IV-1.1	20	0.2110	1.3819	$\pm 0.1818$	3.55
IV-2.0	14	0.2143	1.5219	$\pm 0.0780$	2.86
IV-2.1	15	0.2724	1.5964	$\pm 0.1055$	3.30
$0.38 < \hat{R} < 1.61$	21	0.2326	1.5555	$\pm 0.1837$	3.84
7-Events	97	0.2443	1.3830	$\pm 0.0503$	3.67
5-Events	73	0.2395	1.4556	$\pm 0.0481$	3.13

\*Omitted from 5-Event fit.

IV-2.0, and IV-2.1.

The mass of data from these events (64 of the 97 peak-velocity/range pairs) biases the regression line toward lower decay rates. The regression analysis of single events suggests that the decay rate over the larger range interval may be as high as that for Cowboy. It also shows that data for Events II-7 and IV-1.0 are less consistent than data for the other events; standard deviations are two to four times the next largest values. On the basis of those large uncertainties and the increasing evidence that the unsurveyed charge placement hole for Event II-7 wandered far from its intended location, all records for Events II-7 and IV-1.0 were ignored and a revised linear regression fit derived. The revised fit (shown as 5-Event Fit in Figure 6) is

$$U_{\max} = 0.2395\hat{R}^{-1.456 \pm 0.0480} \quad (6)$$

The standard deviations for  $n$  and  $\log A$  (the decay exponent and logarithm of the amplitude, respectively) and the width of the 90% confidence bounds ( $U^+/U^-$ ) are reduced from the seven-event fit.

To test the Cowboy Trails data for transition to elastic decay over the interval of observation, quadratic regression fits

$$\log U_{\max} = A + B \log \hat{R} + C (\log \hat{R})^2 \quad (7)$$

were obtained. Results for Event III are meaningless since only 4 records are available and the quadratic fit shows decay rate increasing with range ( $C > 0$ ). The nine other cases show decay rate decreasing with range, but the uncertainties in  $A$  and  $B$  [Eq. (7)] (measured by the standard deviation divided by the coefficient) are larger than the corresponding uncertainties in the linear fit. The uncertainty in  $C$  (standard deviation  $\div C$ ) ranges from 0.48 to 10.8. The large standard deviations of the coefficients show only

that there are wide-ranging quadratic fits of almost equal merit (as measured by the least-squares criterion). To get a better idea of the significance of curvature, the standard deviation of the parabola as an estimator of  $U_{\max}$  was compared with that for the linear fit (corrected for the change in the number of degrees-of-freedom). In two of the nine relevant cases of Table 4 (Event III doesn't count) the standard deviation was greater for the quadratic fit than the linear fit. In three cases it was smaller by less than 1%, and in two other cases by only 1.9%. In these seven instances, the fits to Events II-7, IV-1.1, IV-1.0, 7-Events, 5-Events, and Events II-8, and IV-2.1, respectively, there is no substantial evidence that the quadratic is the better fit, i.e., that a transition toward elastic decay takes place as range increases. In the two remaining cases, Event IV-2.0 and the data for the region of overlap with Cowboy, the standard deviation for the quadratic showed net reductions of about 5 and 10%. The quadratic fit for the Cowboy overlap region has an equivalent power law decay ( $\hat{R}^{-n}$ ) that varies from  $n=3.05$  at the inner limit,  $\hat{R}=0.379 \text{ km/kt}^{\frac{1}{3}}$ , to  $n=-0.01$  at  $\hat{R}=1.583 \text{ km/kt}^{\frac{1}{3}}$ , a result at odds with elastic decay ( $n=1$ ) beyond the range interval covered. The results for Event IV-2.0 (with 5% smaller standard deviations than the linear fit) are consistent with transition toward elastic decay for  $\hat{R} > 1.6 \text{ km/kt}^{\frac{1}{3}}$ , the equivalent decay rates ranging from  $n=1.85$  at  $\hat{R}=0.46 \text{ km/kt}^{\frac{1}{3}}$  to  $n=1.15$  at  $\hat{R}=8.47 \text{ km/kt}^{\frac{1}{3}}$ . Overall, however, evidence for a decrease in  $n$  with slant range must be regarded as very weak.

Without additional data, linear regression descriptions of the decay of peak velocity with range,  $U_{\max} = A\hat{R}^{-n}$ , make the most sense. Whether the data are treated by single events or groups of events, the decay exponent  $n$  lies between the value obtained from Cowboy data (1.527) and about 1.35 (our best estimate

being 1.45). There is evidence to support either extreme out to the largest range of observation here. Also, while the data are too scattered to determine whether the decay rate decreases with range, decay is clearly not elastic ( $\propto R^{-1}$ ) even at scaled ranges as great as  $11.3 \text{ km/kt}^{\frac{1}{3}}$ , or seven times the previous maximum scaled range of observation from tamped shots.

### 3.3 Propagation Speed of First Arrivals

In principle, determining first-arrival times is simpler than extracting peak material velocities. It does not depend on exact knowledge of gauge sensitivity or field calibration signal strength, and no geometric correction factors need be applied to account for gauge orientation. All that is required is i) an accurate reference timing signal, ii) accurate location of explosive charges and gauges, and iii) an identifiable first arrival signal. Both accelerometer and velocity gauge signals can be used and the gauges need not function flawlessly after first arrival (till peak velocity or later). In addition, both single-charge and charge-pair events can be used.

In practice, noise often made first-arrival detection difficult in the Cowboy Trails data. More frustrating was the occasional loss of synchronization with the simultaneously recorded IRIGB timing signal which introduced unknown time shifts into a number of record plots. In spite of these difficulties, times-of-arrival were determined for 368 Cowboy Trails records, including records from all events (see Table 5). In several cases, the data suggest otherwise-undetected time-shifts and/or appreciable uncertainties in gauge and charge-location. To exclude the most obvious of these, a wavespeed  $C^*$  was estimated from

$$C^* = r / (t_a - T_0)$$

TABLE 5

Properties of Linear Regression Fits to Time-of-Arrival, Range Data ( $r$ ,  $t_a$ )

$$r = r_0 + Ct_a$$

Event	No. of Points N	Intercept		Wavespeed	
		$r_0$ , m	$\delta r_0$ , m	C, m/ms	$\delta C$ , m/ms
II-7	44	40.502	$\pm 6.617$	4.072	$\pm 0.178$
II-8	23	-4.044	$\pm 2.764$	4.562	$\pm 0.079$
III	25	-0.855	$\pm 1.038$	4.661	$\pm 0.045$
IV-1.0	17	3.374	$\pm 1.902$	4.336	$\pm 0.073$
IV-1.1	59	-3.422	$\pm 1.384$	4.529	$\pm 0.041$
IV-1.2	34	-7.806	$\pm 4.993$	4.859	$\pm 0.159$
IV-2.0	57	-0.512	$\pm 1.081$	4.516	$\pm 0.035$
IV-2.1	8	-2.538	$\pm 1.361$	4.363	$\pm 0.030$
IV-2.2	22	3.058	$\pm 3.204$	4.364	$\pm 0.072$
IV-3	48	-0.440	$\pm 1.084$	4.419	$\pm 0.033$
9 Events (Not II-7)	292	-0.510	$\pm 0.689$	4.479	$\pm 0.021$

If this estimate was between  $3C_0/4$  and  $4C_0/3$ , where  $C_0 = 4.6$  m/ms (the expected wave speed), the data were retained.

Difficulties encountered in drilling the charge emplacement hole and reaming the spherical charge cavity for Event II-7 suggested that the hole had wandered significantly from vertical. Digital data file identification problems had cast doubt on the locations (through gauge identification) of most of the records for Event IV-3 and a few isolated records in other events. As a further test of the validity of the data, regression fits to range as a function of arrival time  $r=r_0 + C(t_a - T_0)$  were obtained for each event, Table 5. Large values of  $r_0$  suggest systematic errors in reported values of the slant range or time of arrival. Large values of the standard deviations of  $r$ ,  $r_0$  and  $C$  suggest random errors. Data from Event II-7 is suspect on both grounds. It also shows a suspiciously low wave speed 4.07 m/ms. All Event II-7 time-of-arrival data was therefore excluded from further analysis.

Data from Event IV-1.2 also shows larger standard deviations and a larger-than-average  $r_0$ . Since there was no other reason to be wary of the data for this event, it was retained. The resulting data set - 292 time-of-arrival, range pairs from nine events - was used to determine the propagation speed for first arrivals,  $4.479 \pm 0.021$  m/ms. The regression fit and all 368 data points are shown in Figure 9.

## SECTION 4

### ANOMALOUS VELOCITY GAUGE SIGNALS

The completed Cowboy Trails instrumentation array should have provided 434 velocity gauge records suitable for determining

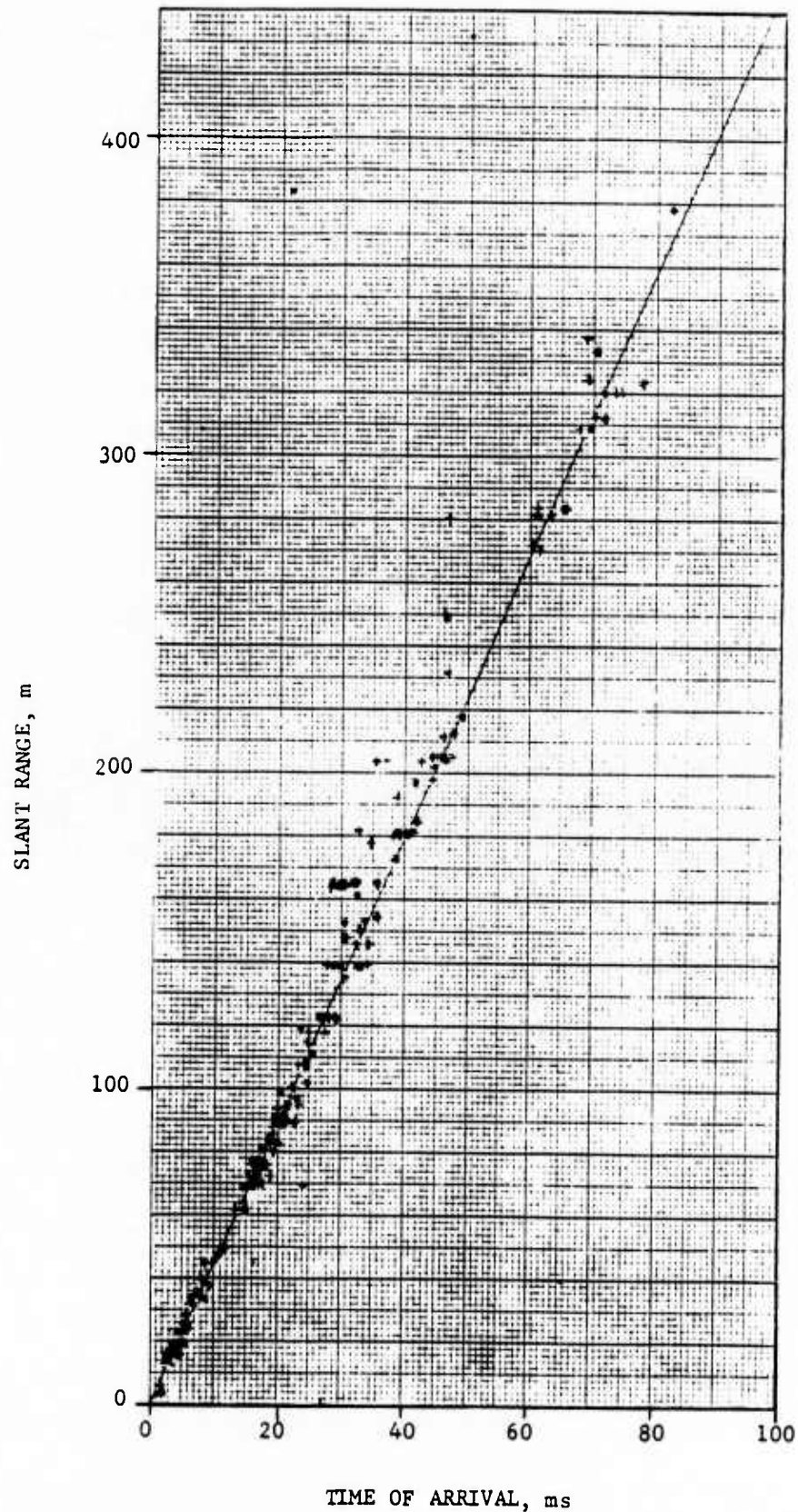


Figure 9. Cowboy Trails: Time-of-Arrival, Range Data. The linear regression line,  $r = r_0 + C_0 t_a$ , is the least-squares fit to 292 points from 9 of the 10 events. It indicates a first-arrival signal speed of  $4.479 \pm 0.021$  m/ms.

radial velocity from the seven single-charge events. Nearly 80% of those records (347) exhibited noise and baseline problems (see Table 2), 56% of them being so severely affected that they were not considered valid through peak velocity. Outright failure of the gauges accounted for the loss of only 75 records. Since the number lost to noise and baseline problems is more than twice the number of records considered good through peak velocity, both with and without simple corrections (117), it made sense to try to remove the anomalies and recover useful data.

#### 4.1 Baseline Drift

The baseline problem was tackled first, because we suspected that the integrator circuit was at fault. Identification of the cause would reveal the steps for its correction in records in hand and for its avoidance in future tests. This same problem was evident in evaluation tests performed by the New Mexico Engineering Research Institute (NMERI)\* for the Air Force Weapons Laboratory.<sup>17</sup> In those tests, gauge output shows the correct boxcar-like velocity pulse superimposed on a linear ramp. In the Cowboy Trails records, the velocity pulses are more complex and the drift rate varies with time. Drift starting times and rate are not revealed by inspection. With the cooperation of the velocity-gauge manufacturer, an unpotted gauge and details of the integrating circuit (shown schematically in Fig. 10) were obtained for laboratory and computational testing. To facilitate electrical measurements, a breadboard mock-up of the integrating circuit was built and tested against the factory specifications and the unpotted factory-built circuit. The breadboard integrator

\*NMERI reports no attempt to determine its cause, reporting only that the gauges "exhibited large baseline shifts (sic)", and "erratic behavior . . . when . . . subjected to cross-axis input."

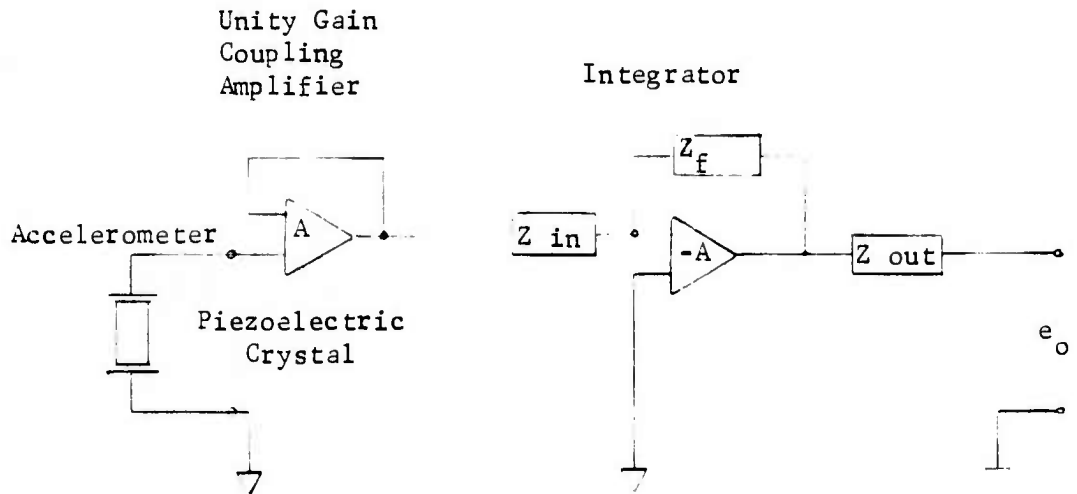


Figure 10. Simplified Schematic Diagram of the Bell & Howell Velocity Gauge. A pulse generator was substituted for the piezoelectric crystal in most of the bench testing.

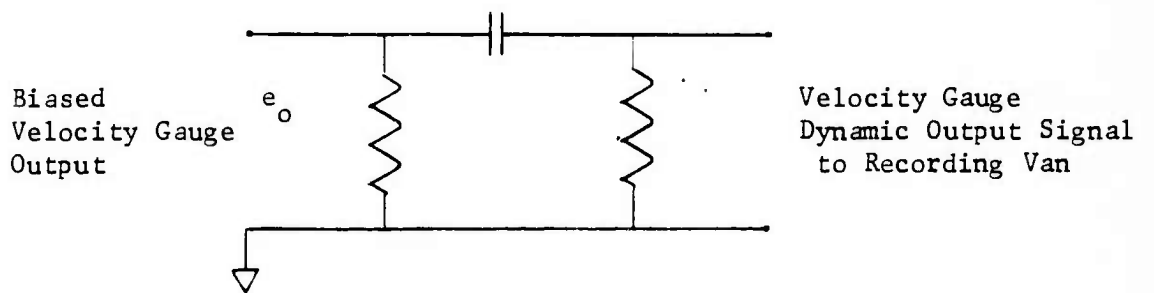


Figure 11. Schematic of the Bias Nulling Circuit for the Bell & Howell Velocity Gauge.

circuit was driven by a pulse generator in place of the piezoelectric accelerometer element (crystal) of the gauge. Once a leaky capacitor had been identified and replaced, the breadboard circuit performed as predicted from the circuit equations.

Laboratory testing of the unpotted gauge required the addition of the bias nulling circuit (Fig. 11) used in the field to remove a 12 volt DC signal superimposed on the dynamic output of the integrator circuit. The pulse generator was also used to drive the factory integrator circuit. When the gain of the nulling circuit was accounted for, the factory integrating circuit performed according to specifications, matching (within a few percent) the breadboard response and calculated response of the circuit equations to steady state sinusoidal input of from 1 to 5000 HZ as shown in Table 6. Higher gains but comparable agreement with calculated response were obtained for single boxcar pulse input, for pulse durations from 1 ms to a few hundred ms.

The integrator circuit was also tested by attaching the piezoelectric accelerometer, shock loading it while monitoring both the accelerometer and integrator circuit output. The accelerometer output pulse (Fig. 12a) was then modelled by superposing 19 boxcar pulses and used to drive the circuit equations. Calculated and measured integrator circuit output pulses are compared in Figure 12b.

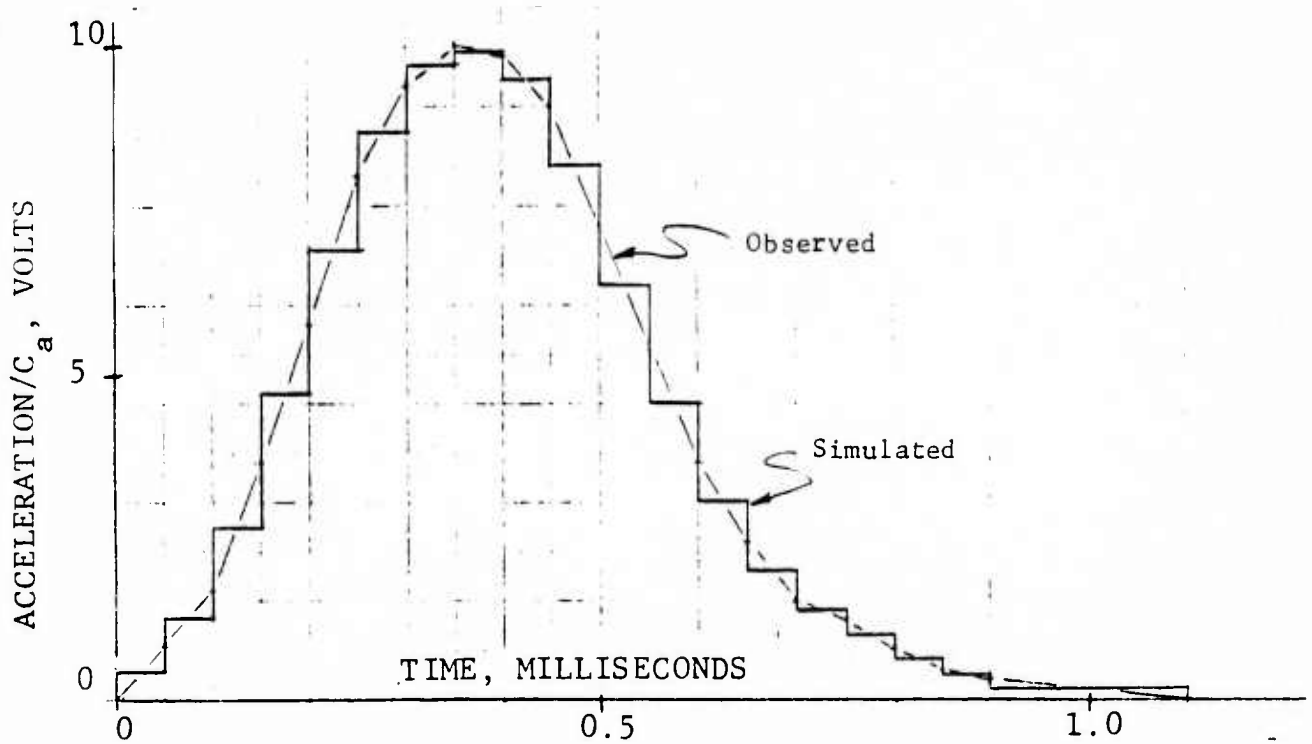
The integrator circuit response was a linear function of input pulse amplitude up to the limiting voltage specified by the manufacturer. At higher input voltages (accelerations beyond the certified operating limit) anomalous integrator output was seen. The anomalies, however, were very different from the behavior noted in the Cowboy Trails data. The accelerometer output voltage and bias-nulled integrator output voltages for an overload test

TABLE 6

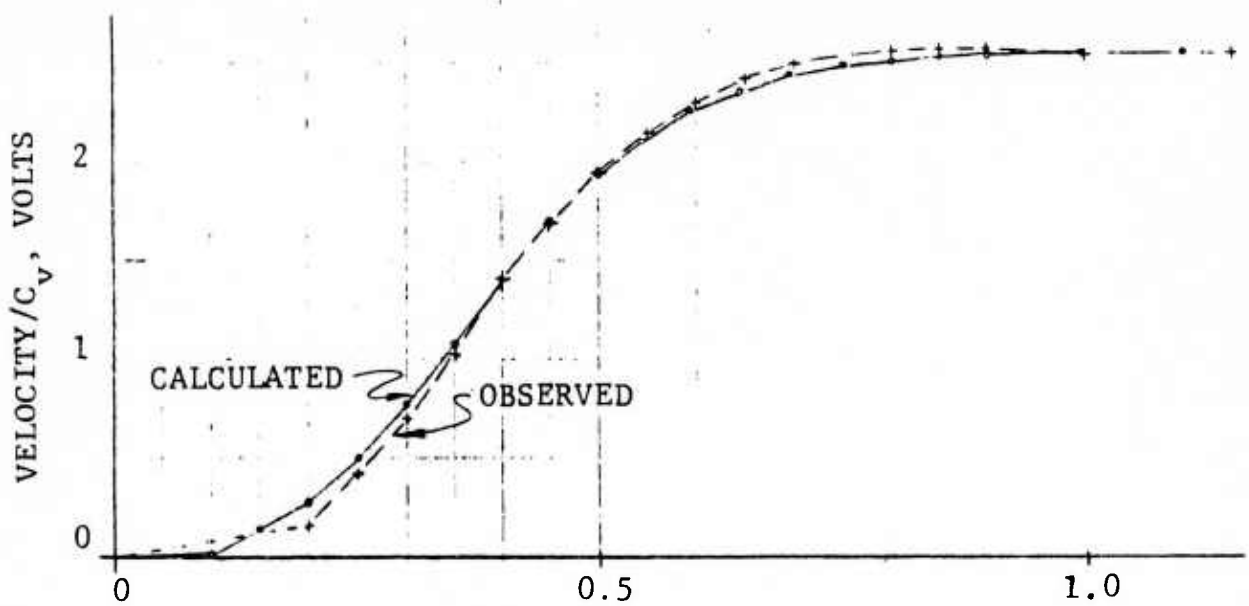
Comparison of Theoretical and Measured Response of the Bell &amp; Howell Integrator Circuit

Frequency, HZ	Integrator Circuit Gain for Sinusoidal Input		
	Theoretical	Breadboard	Factory
1	80.31	82.95	85
2	39.58		44.98
5		15.96	15.4
10	7.88	7.61	8.2
15		5.52	5.33
20	3.94	3.93	4.30
25		3.19	3.23
50	1.58	1.55	1.62
75		1.05	1.07
80	0.984	0.995	1.00
100	0.788	0.795	0.804
250	0.315	0.33*	0.32*
500	0.158	0.16*	0.16*
1000	0.0788	0.08*	0.08*
2000	0.0394	0.043*	0.039
3000	0.0263	0.028*	
4000	0.0197	0.020*	0.019
5000	0.0158	0.016*	0.0128

\*These are single measurements. Other entries for breadboard and factory circuits are averages of two measurements,



a) Accelerometer Stage Output (Integrator Input)



b) Velocity Pulses (Integrator Output)

Figure 12. Comparison of Observed and Calculated response of a Bell & Howell Velocity Gauge to an Observed Acceleration Pulse.

are shown in Figure 13. When the accelerometer crystal output voltage first exceeds 10 volts (the saturation voltage for the unity gain amplifier between the crystal and the integrator circuit in Figure 10) the integrator circuit abruptly ceases to function properly, point A. The subsequent abrupt flattening of the accelerometer output at ~12 volts occurs too late to have triggered the malfunction. It has no visible effect on integrator response. The integrator circuit returns to proper function when the accelerometer voltage drops below 10 volts, point B, but has lost its reference. The output signal is meaningless beyond point A.

The accelerometer stage was also subjected to cross-axis loading - an apparently reliable means of exciting baseline drift in NMERI's evaluation tests<sup>17</sup>. A small spring-driven jiggle table carrying the piezoelectric crystal was moved to one of its extreme positions and released, subjecting the accelerometer stage to a slowly decaying ~30 HZ signal with a peak acceleration of 1 or 2 g's, much lower than the nominal 200 to 1000 g's of the NMERI tests. Velocity signals for both on-axis and cross-axis loading were clean, sinusoidal pulses without baseline drift. Amplitude of the output for cross-axis loading was about 10% of that for on-axis loading.

Based on the long series of bench tests on factory and bread-board integrator circuits, the integrator is clearly not the cause of baseline problems. Within the specified operating limits, its steady state response to sinusoidal input is that computed for the circuit (phase and gain). The circuit is stable, linear, and accurate for single boxcar-pulse and pulse-train input for durations from 0.5 to a few hundred milliseconds and input signal amplitudes less than 10 volts. If baseline drift is the result of a

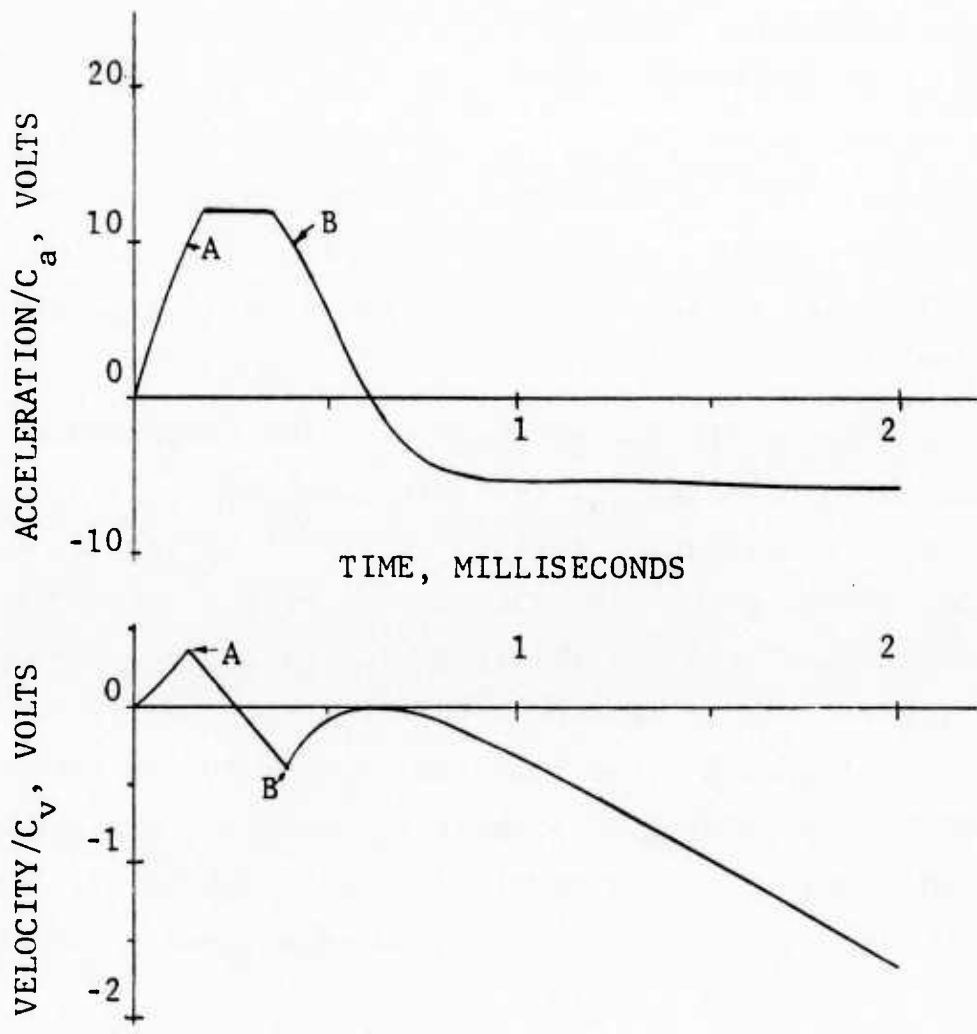


Figure 13. Observed Response of a Bell & Howell Velocity Gauge During Overloading of the Accelerometer Stage.

gauge defect, the defect is not in the integrator circuit. Tests of the accelerometer stage were not complete enough to rule it out as the source of baseline drift problems; amplitudes were much too low. Exposure to the dank, salty atmosphere of the mine which corrosively attacked tools, electronic gear and unprotected circuit connections, may have contributed to the baseline problems of the velocity gauges, but the results of the NMERI tests (not explained) in the benign environment of the laboratory suggest otherwise.

#### 4.2 Noise

During screening and evaluation of the ground motion data for Cowboy Trails, noise frequencies were estimated by counting the number of peaks over time intervals of a few tens of milliseconds. Since the noise signals are not clean sinusoids, the frequencies are only approximate. High voltage spikes in the commercial 60 HZ AC power (the result of a load switching surge) triggered the early firing of the IV-2a charge (Event IV-2.0). As a result, records were expected to show 60 HZ noise and its higher harmonics. Spikey 60 HZ noise (see Figure 14) that nearly obscures the ground motion signal was found in some records.

Examination of the records show noise frequencies of 300 to 600 HZ as well as the expected 60 HZ already noted. Some records show a ringing response to signal arrival, suggesting vibration of a gauge mount or gauge element. Noise bursts and ringing signals showed frequencies of about 1500 HZ. In those instances where a regular pattern of noise can be identified, it appears that signal quality can be enhanced by further processing of the digital records . . . e.g., the use of notch filters to remove narrow-band noise. More complex procedures (signal differencing in

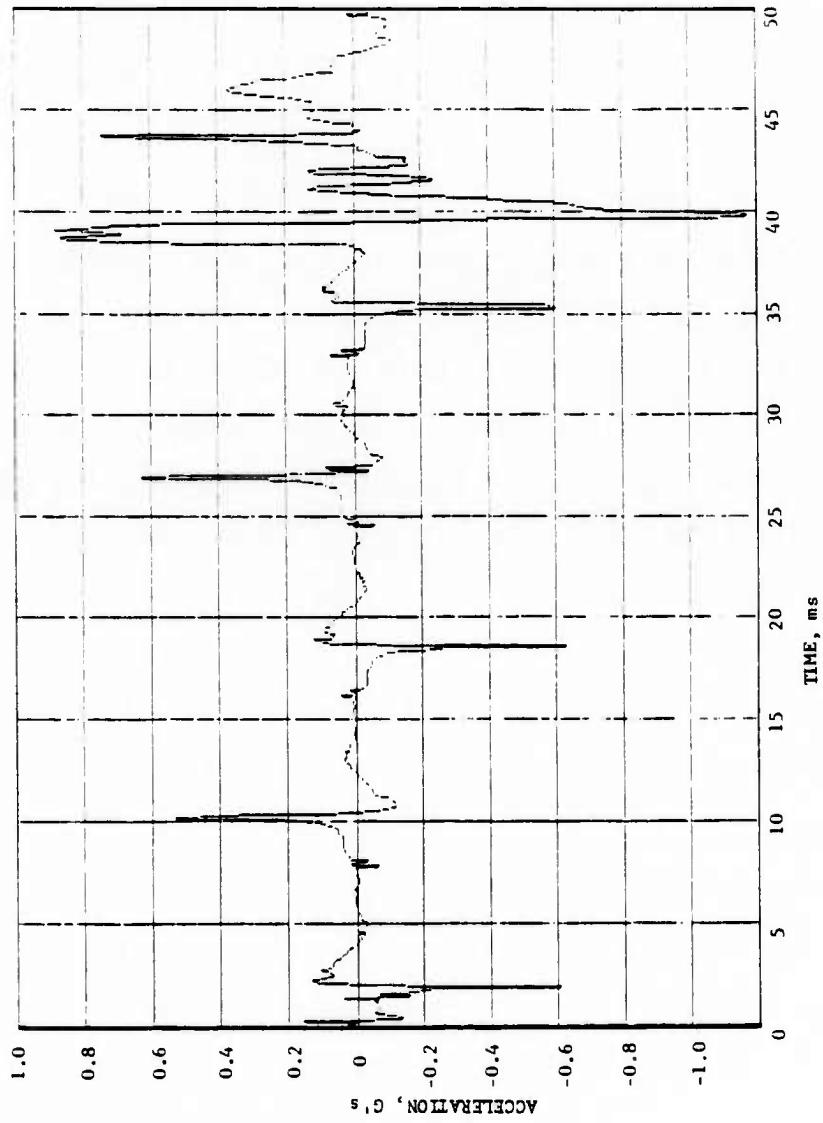


Figure 14. Spikey 60 HZ Noise in a Cowboy Trails Ground Motion Record. In this accelerogram, the noise spikes are nearly as high as the acceleration pulse which arrives at about 39 ms.

transform space) may be required to remove the spikey 60 HZ noise pulses like those seen in Fig. 14.

The techniques for removing noise don't require that the sources of the noise be identified, though that would be helpful in preventing data loss to noise in future events. The suspected sources of noise here are the commercial AC power, shock-induced vibration of gauge mount and gauge elements, corrosion, and differences in the ground potentials in the mine and at the instrumentation van at the ground surface.

## SECTION 5

### CONCLUSIONS AND RECOMMENDATIONS

Ground motion data from single charge events in the Cowboy Trails program show that signal propagation in dome salt is inelastic out to scaled ranges of  $11.3 \text{ km/kt}^{\frac{1}{3}}$ , a range seven times that where good free-field measurement had been made before. Over the scaled range interval  $0.388 < \hat{R} < 11.3 \text{ km/kt}^{\frac{1}{3}}$  peak velocity decayed according to

$$V_{\text{max}} = 0.2395 \hat{R}^{-1.456 \pm 0.048} \text{ m/s}$$

The rate of decay is slightly lower than that observed in Cowboy, but amplitudes are higher by about a factor of two.

Propagation speed for first arrivals from both single-charge and charge-pair events over the scaled range interval  $0.388 < \hat{R}$

$< 9.76 \text{ km/kt}^{\frac{1}{3}}$  was

$$C_0 = 4.479 \pm 0.021 \text{ km/s}$$

in close agreement with the values for Cowboy (4.5 km/s average<sup>18</sup> from shot data,  $4.374 \pm .03$  km/s from seismic survey<sup>19</sup>) and Salmon ( $4.699 \pm .025$  km/s from shot data,  $4.507 \pm .135$  from uphole survey, and  $4.516 \pm .045$  from cross-hole survey<sup>1</sup>).

These results are based on a small fraction of the records obtained . . . 73 of 514 velocity records and 292 of 625 times-of-arrival. Analysis of subsets of data (i.e., data for separate events) led to the exclusion of all time-of-arrival and velocity data for Event II-7. A large error in source location, hinted at by difficulties in the drilling and reaming operations, was apparent in the time-of-arrival analysis and in the fit to peak velocity, range data. Peak velocity data from Event IV-1.0, the result of the first misfire of a charge-pair event, was also excluded on the basis of standard deviations substantially larger than those for fits to other events. Baseline drift and noise were severe enough in 325 records to render them invalid for determining peak velocity. The inability to reliably separate pulses from the two charges in Event IV-1.2, IV-2.2 and IV-3 and large apparent errors in the locations of charges IV-2.2a and IV-3a led us to forgo use of charge-pair data in assessing peak velocities from single charges. Ambiguity in the azimuthal coordinate for canisters C3 through C11 clouded the data from those gauges in all but Event III through an orientation uncertainty of about 16 degrees. Locations for those canisters were uncertain by about 20% of slant range from Event III charge. In spite of all these difficulties the data show a high degree of consistency in both peak velocity as a function of range

and first-arrival speed. It therefore seems clear that further effort to recover data from the flawed records, and to reduce uncertainties in configuration, would be worthwhile.

Specific recommendations follow:

1. Perform laboratory tests of the piezoelectric integrating accelerometer to determine the cause of baseline drift.
2. Correct velocity pulses from the 300 records affected by baseline problems, using results of the baseline drift tests in conjunction with digital data processing techniques.
3. Try removing noise from the accelerometer and velocity gauge records by such means as spectral analysis and narrow-band filtering.
4. Reduce the uncertainty in the location of the charge for Event II-7 inverting time-of-arrival data, using the first arrival wave-speed and gauge stations with well-established positions. The slant-range uncertainty for canisters along C-line is probably too small ( $< 10$  m) to be resolved in a similar way.
5. Integrate the accelerometer records correcting first for non-spherical orientation. Compare with corresponding velocity records to establish the relative performance of the two gauges (accelerometer and integrating accelerometer) if unambiguous access to the digital records can be obtained.
6. Redigitize velocity and accelerometer data in events where many records remain inaccessible due to uncertain identification, uncertain reference time, or digital tape read-write problems.
7. When corrections for baseline, noise and as-built geometry have been completed and the technical problems of digital record identification and access resolved, pass the Cowboy Trails

records through filters representing the Cowboy gauge frequency response characteristics.

8. Continue to develop displacement gauges. Accurate measurement of displacement at one or more times establishes a benchmark for correcting baseline problems in velocity and acceleration.

## REFERENCES

1. Perret, W. R., "Free-Field Particle Motion from a Nuclear Explosion in Salt, Part I; Vela Uniform Program, Project Dribble, Salmon Event," VUF-3012, Sandia Laboratory, November 1967.
2. Murphey, B. F., "Project Cowboy: Particle Motions Near Explosions in Halite," SC4440(RR), Sandia Corporation, June 1960.
3. Trulio, J. G., "Simple Scaling and Nuclear Monitoring," ATR-77-45-2, Applied Theory, Inc., April 1978.
4. Trulio, J. G., "Cowboy Trails, Phase I: Small-Scale Explosive Tests in Salt Domes, Part I Goals, Methods and Conclusions," ATR-83-53-1, Applied Theory, Inc., 15 June 1983.
5. Vincent, C. T., et al., "Phase II Field Data Report," PAI-FR-0118, Physics Applications, Inc., October 1983.
6. Ford, F. C., and Vincent, C. T., "Planning Phase III Effort for Chemical Explosions in Salt in Support of the ATI Ground Motion Prediction Program," PAI-FR-3, Physics Applications, Inc., July 1980.
7. Vincent, C. T., et al., "Phase III & IV Field Data Report," PAI-FR-0119, Physics Applications, Inc., October 1983.
8. Barker, T. G., "Surface Recordings of PAI Phase II Explosive Tests," Systems, Science and Software, VSC-TR-82-27, April 1982.
9. Keough, D., "Stress Measurement During Cowboy Trails," Stanford Research Institute, April 1984.
10. Trulio, J. G., "Preliminary Results of the Grand Saline Experiment," Presentation File No. 101, presented at 5th Annual DARPA/AFOSR Symposium on Seismic Research Rosario Resort 16-18 May 1983, Applied Theory, Inc., May 1983.
11. Vincent, C. T., "Cowboy Trails Phase III & IV Field Notebook," Physics Applications, Inc.
12. Vincent, C. T., Private Communication to J. W. Workman.
13. Hake, L., "High Explosives, Arming and Systematics," SC4833 (RR) Sandia Corporation Livermore Laboratory, (undated).
14. Workman, J. W., Trulio, J. G., and Stokes, E. S., "In-Situ Explosions: Strain Fields Calculated from Measured Velocity Pulses," SAMSO-TR-78-126, Applied Theory, Inc., August 1978.

15. Thornbrough, A. D., Ames, E. S., and Hawk, H. L., "Instrumentation Systems - Project Cowboy," SC-4470(RR) (Supplement to SC4440(RR)) Sandia Corp., September 1960.
16. Perl, N. K., Applied Theory, Inc., Private Communication to J. W. Workman, February 1985.
17. Noble, C. D., "Piezoelectric Integrating Accelerometer Evaluation," New Mexico Engineering Research Institute, AFWL-TR-81-140, December 1981.
18. Trulio, J. G., Bless, S. T., and Voland, G. G., "Isotropy of Natural Salt: Implications of Underground Explosive Testing," ATR-74-41-1, Vol II, Applied Theory, Inc., September 1975.
19. Nicholls, H. R., Hooker, V., and Duvall, W. I., "Dynamic Rock Mechanics Investigations: Project Cowboy," APRL-38-3.2, U. S. Bureau of Mines Applied Physics Research Laboratory, 1 September 1960.

## APPENDIX A

### THE PLANNED COWBOY TRAILS PROGRAM

#### A.1 Program Objectives

The program's primary objectives were to

- a) Measure a nearly-spherical seismic source driven by a contained explosion;
- b) Determine an actual spectrum of NE-CE equivalence factors;
- c) Determine the site-to-site variability of explosively-driven motion in "one" medium;
- d) Determine the accuracy of simple scaling rules from lab yields ( $10^{-8.3}$  kt) to that of Salmon ( $10^{.7}$  kt).

The program also had a set of secondary objectives, namely, to

- e) Measure the variation of the field with overburden;
- f) Measure the energies of common and promising CE's;
- g) Measure the effect of charge-shape on the field;
- h) Measure permanent displacement,  $D_{\infty}$ , vs. slant range; from those data, determine the actual drift of ground-motion gauges and show how to correct for it.

In addition, the program served almost inevitably some ancillary objectives that hold broad interest; these were to

- i) Test low-cost CE's for reproducibility;
- j) Determine how feasible it is to use cavities formed by CE in place of NE-formed cavities, as charge-holes;
- k) Determine the suitability of explosively-formed

cavities as charge-holes for tamped and decoupled shots ("cheap mining");

1) Test stress gauges.

## A.2 The Program

The program visualized to gain these objectives, which are all experimental, hinges on a series of experiments requiring only post-shot measurements (Phases I and II of the program) and another series in which motion is measured dynamically (Phases III and IV).

I. The following scheme was proposed to determine the influence of major variables on cavity size:

a. Charge Shape - Compare volumes of cavities from lab shots with cylindrical charges of average COWBOY shape, and with spherical charges, in pressed salt and also in blocks of Grand Saline salt. If the need arises, fire a COWBOY-like charge weighing ~180 lbs in the Grand Saline dome, as an addition to Phase II.

b. Overburden - Compare the shapes and sizes of Phase II cavities; overburden is to vary from 40 to 100 bars in Phase II. Also, compare the shapes and sizes of cavities from lab shots in pressed salt, and again from lab shots in blocks of Grand Saline salt (60-to-350 bars of confining pressure).

c. Site - Compare COWBOY and Phase II cavities, corrected for charge-shape (Ia, above), to get a direct measure of the differences between salt domes as explosion sites (overburden, yield and even explosive, can be held constant in that comparison). Compare cavities left by lab shots in pressed salt, with those left by lab shots in blocks of Grand Saline salt. Compare the latter cavities

with Phase I cavities to detect differences between laboratory and in-situ behavior of Grand Saline salt.

d. Scale - Compare cavities from Phases I and II, correcting (if necessary) for the small difference in overburden (Ib, above).

## II. Influence of Major Variables on Free-Field Motion:

a. Charge Shape - In the laboratory, fire cylindrical charges of average COWBOY shape, and spherical charges, in both pressed salt and blocks of Grand Saline salt. If the need arises, fire a charge of each shape in its own block of dome salt - or even a COWBOY-like cylindrical charge (~180 lbs), at Grand Saline.

b. Overburden - Compare motions from Phase III and a deep shot in Phase II; the overburden variation should be ~40 bars. Compare motions from lab shots in pressed salt at confining pressures from 0 to 50 bars, and again at confining pressures of 40, 100 and 180 bars in blocks of Grand Saline salt.

c. Site - Compare COWBOY and Phase III motions, corrected for charge shape (IIa, above), to obtain a direct comparison between salt domes (yield and overburden are very nearly the same for COWBOY and Phase III). Also, fire lab shots in pressed salt and dome-salt, to see how motions differ in salt media created by different processes.

d. Material Hardening - Compare motions measured in Phases III and IV to detect any systematic change in the free field driven by a single spherical charge, as the number of previous shots grows (e.g., the medium could become noticeably more elastic).

e. Scale - Lab shots in blocks of Grand Saline salt (6-10 gms of CE), the Phase III shot in the Grand Saline dome (180 lbs of CE), and SALMON (5.3 kt; NE) determine the effects of scale on free-field motion over nine orders of magnitude in yield. The lab and

Phase III shots are fired in the same medium at the same overburden (~60 bars), but the SALMON shot was fired in the Tatum dome at an overburden of ~180 bars; corrections for those differences are made to SALMON data using results obtained in this program on the effects of site and overburden variations (IIb. and c., above). Little would be gained by comparing adjusted SALMON pulses in all detail with lab pulses and Phase III pulses, because NE and CE differ too greatly. Instead, in comparing fields driven by different types of explosive, define scale effects in terms (for example) of rates of decay of peak velocity and displacement with respect to slant-range. SALMON and COWBOY pulse-shapes proved similar enough to justify such comparisons.

### III. Seismic Sources and NE-CE Equivalence. -

a. Seismic Source Created by NE - From the pulses of Phase III, construct a complete spherical velocity field for that event over its instrumented slant-range-interval (the "baseline spherical field"). Do likewise for SALMON, and extrapolate the SALMON field outward in range until the lowest Phase III amplitudes are reached; to extrapolate, apply to SALMON the factors that define changes in pulse-shape and amplitude in the baseline field, during whose construction those factors are found. Then, after correcting superposition-data from Phase IV for the effects of prior shots, identify a minimum slant-range, or "linear radius", beyond which waves from a single CE charge propagate in linear fashion. As the linear radius for SALMON, take the slant-range at which both (i) the amplitude of the SALMON velocity pulses is at least as low as in the Phase III field at its linear radius, and (ii) over the frequency band of interest in nuclear monitoring, logarithms of RVP-spectral amplitudes decay at the same rates in the two fields.

b. Seismic Source Created by CE - Phase III motion at the linear radius found in Phase IV (IIIa, above) is the seismic source for chemical explosions in salt.

c. NE-CE Equivalence - Bring the baseline spherical field (IIIa, above) and the extended SALMON field to a common yield, overburden and dome by adjusting either field or both for changes in scale, overburden and site (the adjustment is made in accord with previous results; IIb, c and e, above). From RVP-spectra of the resulting CE- and NE-driven fields, compute equivalence-factor spectra for both phase and amplitude. Do likewise for other yields, burial depths and domes, if the effects of changes in scale, overburden or site on the simply-scaled baseline field have been found significant.

### A.3

A flow diagram showing how the measurements made in each phase of the program contribute to achieving its goals is shown below in Fig. A. To explain how the diagram works, suppose one asks how the effects of scale on the free field are determined in the program. The answer is found by tracing backward from the input to "SCALE" (for the free field), which quickly branches in three directions. One branch leads back to "BASELINE SPHERICAL FIELD" [obtained in Phase III] and "PELLETOL ENERGY" [obtained by combining data from Phases I and II]. Another branch leads directly back to the FREE FIELD obtained for DOME SALT in Lab Shots. The third branch leads back to a node; there data from SALMON are combined with data on the change in free field with SITE and OVERBURDEN. Thus, shots at lab scale (6-10 gms of CE), mine scale (180 lbs of CE) and the Salmon shot (5.3 kt; NE) are the sources of data as

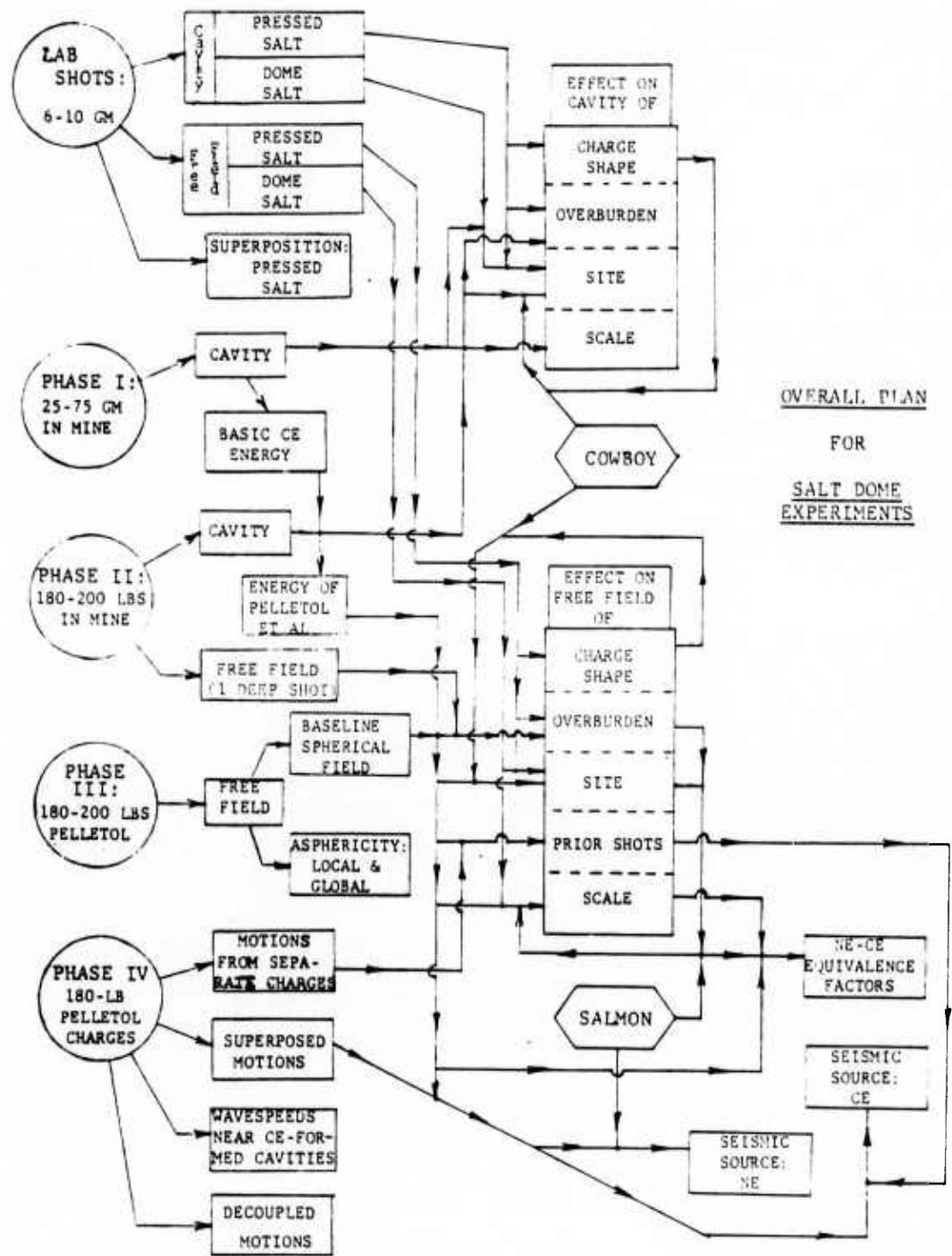


Figure A. Overall Plan for Salt Dome Experiments

to the effects of scale on free-field motion in the Grand Saline dome - and since the Salmon burst occurred relatively deep in the Tatum dome, corrections for changes in overburden and dome are first applied to Salmon data, in accord with results obtained earlier in the program.

Caveats are not covered by the Diagram: Salmon motion, driven by NE, can only be compared in a limited way with the CE-driven motions at lower yields. Since pulse-shapes are similar in CE and NE bursts (witness Salmon and Cowboy), it will probably be most fruitful to compare rates of decay of peak velocity and displacement with slant-range. By all odds, the best way to evaluate scale effects over the wide yield-interval between Salmon and 180 lbs. of Pelletol, is to detonate a large charge of CE (500 tons, say) in a dome. Such a shot would leave almost no uncertainty in either scaling or NE-CE equivalence - and has therefore been part of ATI's suggested plan from the start. Also, while Lab Shots will be fired in blocks of Grand Saline salt at about the same confining pressure as in the mine, the blocks are disturbed during their removal. To account for the effects of that disturbance, it should suffice to fire shots in blocks of different size.